A Cl^- Cotransporter Selective for NH_4^+ Over K^+ in Glial Cells of Bee Retina

Païkan Marcaggi* and Jonathan A. Coles*‡

From the *Institut National de la Santé et de la Recherche Medicale U394 Neurobiologie intégrative, Institut François Magendie, 33077 Bordeaux cedex, France; and ‡Institut National de la Santé et de la Recherche Medicale U438 RMN Bioclinique, CHU Grenoble, 38043 Grenoble cedex 09, France

abstract There appears to be a flux of ammonium (NH_4^+/NH_3) from neurons to glial cells in most nervous tissues. In bee retinal glial cells, NH_4^+/NH_3 uptake is at least partly by chloride-dependant transport of the ionic form NH_4^+. Transmembrane transport of NH_4^+ has been described previously on transporters on which NH_4^+ replaces K^+, or, more rarely, Na^+ or H^+, but no transport system in animal cells has been shown to be selective for NH_4^+ over these other ions. To see if the NH_4^+-Cl^- cotransporter on bee retinal glial cells is selective for NH_4^+ over K^+ we measured ammonium-induced changes in intracellular pH (pH_i) in isolated bundles of glial cells using a fluorescent indicator. These changes in pH_i result from transmembrane fluxes not only of NH_4^+, but also of NH_3. To estimate transmembrane fluxes of NH_4^+, it was necessary to measure several parameters. Intracellular pH buffering power was found to be 12 mM. Regulatory mechanisms tended to restore intracellular $[H^+]$ after its displacement with a time constant of 3 min. Membrane permeability to NH_3 was 13 $\mu m\ s^{-1}$. A numerical model was used to deduce the NH_4^+ flux through the transporter that would account for the pH_i changes induced by a 30-s application of ammonium. This flux saturated with increasing $[NH_4^+]_o$; the relation was fitted with a Michaelis-Menten equation with $K_m \approx 7$ mM. The inhibition of NH_4^+ flux by extracellular K^+ appeared to be competitive, with an apparent K_i of ~15 mM. A simple standard model of the transport process satisfactorily described the pH_i changes caused by various experimental manipulations when the transporter bound NH_4^+ with greater affinity than K^+. We conclude that this transporter is functionally selective for NH_4^+ over K^+ and that the transporter molecule probably has a greater affinity for NH_4^+ than for K^+.

key words: ammonia • K-Cl cotransporter • neuroglia • pH • Apis

INTRODUCTION

Although transmembrane transport of ammonium in animals has been studied, mainly in the mammalian kidney, there are two well-established cases of fluxes of ammonium from neurons to glial cells in nervous tissue. In vertebrate brain, where glutamate is the main neurotransmitter, the uptake of glutamate by astrocytes followed by its amination to glutamine, which is returned to the neurons and deaminated, implies a flux of ammonium (Benjamin and Quastel, 1975; Hassel et al., 1997). In bee retina, the main metabolic substrate of the neurons (photoreceptors) is alanine formed by amination of pyruvate in the predominant glial cells ("outer pigment cells"). The alanine is transferred to the photoreceptors and deaminated to pyruvate and the tissue releases ammonium (Tsacopoulos et al., 1994, 1997b; Coles et al., 1996).

Uptake of ammonium into cells can be monitored continuously, but indirectly, by measuring the changes in intracellular pH (pH_i) that it causes. Ammonium has a pK_a of ~9.2 in water (Sillén, 1964) so that at physiological pH (in the range 6.5–7.5) a fraction in the order of 1% is in the neutral NH_3 form. Nearly all cell membranes are permeable to NH_3 (but see Singh et al., 1995), so, when ammonium is applied outside a cell, NH_3 diffuses into it, combines with H^+, and tends to raise pH_i (Jacobs, 1940). In contrast, in astrocytes cultured from neonatal mouse, application of ammonium lowers pH_i because there is an influx of NH_4^+ whose effect on pH_i outweighs the effects of NH_3 fluxes (Nagaraja and Brookes, 1998). The glial cells in slices of bee retina also take up NH_4^+ (Coles et al., 1996), an observation that has been confirmed and extended on bundles of glial cells freshly dissociated from adult retinas (Marcaggi et al., 1999). Application of ammonium causes a fall in pH_i that requires the presence of external Cl^- and is blocked by loop diuretics such as bumetanide (Marcaggi et al., 1999). These observations suggest that NH_4^+ enters the glial cells by cotransport with Cl^- on a transporter with functional similarities to the cation–chloride cotransporters present on many types of cells. The transport on the bee glial cells is not blocked in the absence of Na^+ (Marcaggi et al., 1999), indicating that the transport is of the K^+-Cl^- class rather than the Na^+-K^+-$2Cl^-$ class (see Race et al., 1999).

Several cases have been described of cation-chloride

Dr. Marcaggi's present address is Department of Physiology, University College London, London WC1E 6BT, UK.

Address correspondence to Dr. Païkan Marcaggi, Department of Physiology, University College London, Gower Street, London WC1E 6BT, UK. Fax: 0044 171 413 8395; E-mail: p.marcaggi@ucl.ac.uk

The online version of this article contains supplemental material.

cotransporters, particularly in kidney, being able to transport NH_4^+ in the place of K^+, although with a lower affinity (Kinne et al., 1986). However, in plant roots, transporters are known that are selective for NH_4^+ over K^+ (e.g., Kaiser et al., 1998) so such selectivity is a demonstrated biological possibility. We have found that uptake of NH_4^+ by the transporter in bee retinal cells is only moderately affected by external $[K^+]$. This suggested that the transporter might be the first to be described in an animal cell that is selective for NH_4^+ over K^+ and prompted us to make a quantitative estimate of its selectivity.

Influx of NH_4^+ into a cell is generally associated with transmembrane fluxes of NH_3 (Boron and De Weer, 1976; see Fig. 2 C), so the relation between changes in pH_i (ΔpH_i) and NH_4^+ flux (F_{NH4})[1] is complex. We tackled the question of the NH_4^+/K^+ selectivity in two stages. First, we deduced F_{NH4} from ΔpH_i for relatively brief applications of ammonium. This required accurate absolute measurements of pH_i and measurement of several other parameters: membrane permeability to NH_3, intracellular buffering power, and the kinetics of pH_i regulation. Use of this "cell model" showed a functional selectivity for NH_4^+ over K^+. We then recorded pH_i responses to longer and more complex NH_4^+ application protocols. By simulating these responses with a standard minimal model for a cotransport process, to which we added competitive inhibition, we estimated the NH_4^+ and K^+ affinities of the transporter molecule.

MATERIALS AND METHODS

Intracellular pH (pH_i) in bundles of glial cells dissociated from the retina of the drone (male) *Apis mellifera* was measured by techniques developed from those described in Marcaggi et al. (1999). One record is shown (see Fig. 9 D) from an intracellular microelectrode recording of glial membrane potential in a slice of retina prepared and superfused with oxygenated Cardinaud solution, as described previously (e.g., Coles et al., 1996). Unless otherwise stated, results are given as mean ± SD and the two-tailed paired *t* test was used to determine *P* values. Errors of quotients were estimated by the calculus of errors (Abramowitz and Stegun, 1965).

Dissociation Procedure and Loading of the Cells

Bees were obtained from A. Dittlo (Villandraut) or J. Kefuss (Toulouse, France) and maintained on sugar water. A slice of drone head ~500-μm thick was cut with a razor blade. The slice was incubated for 40 min in a 1.5 ml Eppendorf tube containing 1 ml oxygenated Cardinaud solution (see below) to which had been added 2 mg trypsin (T- 4665; Sigma-Aldrich). The slice was washed in Cardinaud solution lacking Ca^{2+} and Mg^{2+} and the retinal tissue dissected out and triturated. 150 μl of cell suspension was placed in the perfusion chamber (see below) whose floor consisted of a microscope cover slip coated with poly-l-lysine. The cells were allowed to settle for 10 min and then exposed to the acetoxymethyl ester of 2′,7′-bis(2-carboxyethyl)-5(6)-carboxyfluorescein (BCECF-AM) (Molecular Probes, Inc.) at a concentration of 10 μM for 40 min.

Measurement of Fluorescence

The chamber was placed on the stage of an inverted microscope (Diaphot; Nikon) equipped with a 40× objective, photomultiplier detection, and dual wavelength excitation at 440 and 495 nm switched by liquid crystal shutters, as described in Coles et al. (1999). The stimulating light intensity was attenuated so that fluorescence from a bundle of loaded glial cells excited at 440 nm gave a signal of ~10,000 photon counts s^{-1}, which remained stable for several hours. Dark noise plus autofluorescence from a bundle of unloaded cells was <2,500 photon counts s^{-1} for both excitation wavelengths and it was checked that this fluorescence was not affected by ammonium superfusion ($n = 4$). This background fluorescence was automatically taken into account in the in situ pH calibration of each cell bundle (see below). The excitation pattern was usually: 440 nm, 100 ms; off, 20 ms; 495 nm, 600 ms; off 20 ms. To minimize the noise of the ratio, the signal resulting from excitation near the isosbestic point (440 nm) was averaged over several minutes before the PC computer calculated the ratio using a program available from Jean-Louis Lavie (University Bordeaux, Bordeaux, France).

Solutions

The standard perfusion solution contained (mM): 200 NaCl, 10 KCl, 4 $MgCl_2$, 2 $CaCl_2$. pH was buffered with 10 mM MOPS hemisodium salt and set to 6.90 with HCl. Osmolality was adjusted to 685 mOsm with mannitol (~240 mM). The salt components, the pH, and the osmolarity of this solution are similar to those measured in vivo (Cardinaud et al., 1994). For other pHs, PIPES, MOPS, or HEPES were used for solutions of pH 6.20–6.50, 6.90–7.50, or 7.70, respectively. Most other variants were obtained by equimolar replacement of NaCl (or by increasing [NaCl] when [KCl] was reduced). Chloride-free solutions were made by replacing Cl^- by an equivalent quantity of gluconate and increasing Ca^{2+} to 8 mM to counteract the chelating effect of gluconate (Kenyon and Gibbons, 1977). To test the sensitivity of the responses to ammonium to changes in the osmolarities of solutions, osmolarity was intentionally increased or decreased by 5% (~34 mOsm) by changing the concentration of mannitol. Such a change in osmolarity had in itself a barely detectable effect on the emission ratio and no detectable effect on the pH response to 2 mM ammonium ($n = 3$). Therefore, in some experiments, salts such as NH_4Cl were simply added to solutions to final concentrations up to 5 mM without a compensatory reduction in [NaCl].

Perfusion System

To be able to make sufficiently rapid solution changes without detaching the cells from the floor of the chamber, we developed a perfusion chamber with no eddy currents. A factor that appeared to be important was the presence of a curved junction between the floor and the wall of the channel (Fig. 1 A). Solutions were gravity fed and selected by computer-controlled solenoid valves whose outflows passed through fine tubes at ~30 μl s^{-1} into a common pathway to the chamber. It was found that mixing of solutions was negligible. We obtained a measure of the speed of the solution change in the chamber by recording the change in fluorescence during a switch from standard solution to one containing 1 μg $liter^{-1}$ fluorescein (Fig. 1 B). The change in pH_i measured with BCECF in response to propionate or trimethy-

[1]*Abbreviations used in this paper:* BCECF-AM, acetoxymethyl ester of 2′,7′-bis(2-carboxyethyl)-5(6)-carboxyfluorescein; F_{NH4} (and F_{NH3}), transmembrane fluxes of NH_4^+ (and NH_3) per liter of cell; TMA, trimethylamine.

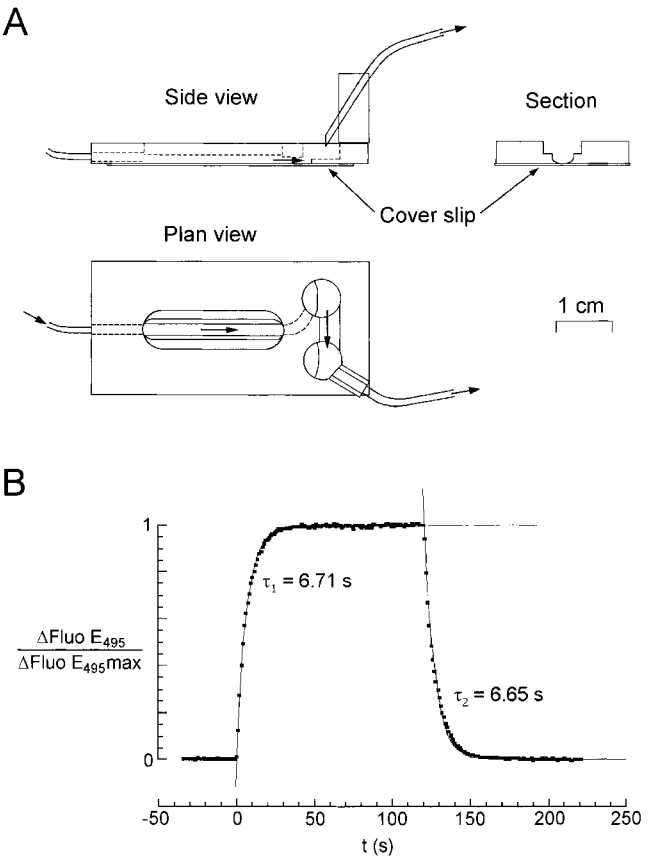

Figure 1. Speed of the solution changes. (A) The perfusion chamber. A channel was milled in a polymethacrylate slab and a glass cover slip was glued on the bottom. Note the rounded edges of the channel. (B) Speed of solution change. The data points show the change in fluorescence observed through the 40× microscope objective focused on cells on the floor of the chamber during a 120-s perfusion change from standard solution to one containing 1 μg liter^{-1} fluorescein. The time scale was displaced so that zero coincides with the beginning of the fluorescence change. The solid lines represent the best fits of data points obtained by regressions with simple exponentials $\{1 - \exp(-t/\tau_1)$ and $\exp[-(t - 120)/\tau_2]\}$ whose time constants, τ_1 and τ_2, are given in the figure.

lamine (TMA) was nearly as fast (see Figs. 4 B and 5 A). The change in fluorescein fluorescence was well described by an exponential; for flow rates used in experiments with cells, the mean time constant was: 5.4 ± 1.9 s (± SD, $n = 16$), and this exponential was used to describe the changes in extracellular concentration in our numerical models.

Calibration of pH_i Measurements

We initially used two techniques for calibrating pH_i. To estimate the shape of the curve that gives pH_i as a function of I_{440}/I_{495}, the cell membranes were made permeable to H^+ with nigericin so that pH_i varied with pH_o (Thomas et al., 1979). At the end of each of 11 experiments, the cells were superfused with 130 mM K^+ Cardinaud solution. Perfusion was stopped and nigericin was added to the chamber to a final concentration of 10 μM. After 10 min, cells were quickly superfused with 130 mM K^+ Cardinaud solutions at different pHs. It was found that the effect of the nigericin persisted so that it was unnecessary to include it in the calibration solutions: there was no significant difference between calibration curves obtained with solutions containing 5 μM nigericin ($n = 4$) and those obtained without ($n = 7$). The value of I_{495}/I_{440} corresponding to pH 6.84 ($[I_{495}/I_{440}]_{6.84}$) was estimated by linear interpolation for each of the 11 data sets. I_{495}/I_{440} was described by the equation of Boyarsky et al. (1988) (Eq. 1):

$$\frac{I_{495}}{I_{440}} = \left[\frac{I_{495}}{I_{440}}\right]_{6.84} \times \left[1 + b\left(\frac{10^{(pH-pK)}}{1+10^{(pH-pK)}} - \frac{10^{(6.84-pK)}}{1+10^{(6.84-pK)}}\right)\right]. \quad (1)$$

The values obtained for the constants were 6.93 ± 0.03 for pK and 0.991 ± 0.022 for b ($n = 11$). The advantage of this procedure is that calibration for each experiment is reduced to obtaining the fluorescence ratio corresponding to pH_i 6.84. This ratio was obtained by superfusing the cells with 2 mM NH_4^+ at pH_o 6.90, a procedure that we found to give a $pH_i \approx 6.84$ (see Fig. 3, A–D).

Absolute Measurement of pH_i

The null method of Eisner et al. (1989) was used. Let $\Delta^a pH_i$ be the change of pH_i that would have been produced by superfusion with a concentration ^aC of a weak acid AH + A^- and $\Delta^b pH_i$ that for a concentration ^bC of a weak base BH^+ + B. Assuming that the diffusion of the neutral form (AH or B) and its re-equilibration with the charged form in the cell are rapid compared with pH_i regulatory mechanisms, then:

$$\Delta^a pH_i \approx -{}^aC \times ([H^+]_o/[H^+]_i)/\beta_i \quad (2a)$$

$$\Delta^b pH_i \approx {}^bC \times ([H^+]_i/[H^+]_o)/\beta_i, \quad (2b)$$

where β_i is the buffering power. Let ΔpH_i be the net pH_i change produced by a simultaneous application of a concentration ^aC of AH + A^- and ^bC of BH^+ + B. $\Delta pH_i = \Delta^a pH_i + \Delta^b pH_i$.

When $\Delta pH_i \approx 0$, it follows from Eqs. 2a and 2b that:

$$[H^+]_i^2 \approx [H^+]_o^2 \times {}^aC/{}^bC$$

$$\text{so, } pH_i \approx pH_o \times 0.5\log({}^bC/{}^aC). \quad (3)$$

To determine the ratio $^bC/^aC$ for which $\Delta pH_i \approx 0$, two pairs of concentrations (^aC; $^bC1$) and (^aC; $^bC2$), which gave rise to ΔpH_i1 and ΔpH_i2 were applied successively. The desired ^bC was then estimated from:

$${}^bC = {}^bC1 \times \left[1 - ({}^bC2 - {}^bC1) \times \frac{\Delta pH_i1}{\Delta pH_i2 - \Delta pH_i1}\right] \quad (4)$$

This method is most accurate when $^bC/^aC = 1$ and hence when $pH_i = pH_o$; we were able to bring pH_i close to pH_o by applying NH_4^+ (see Fig. 3, A–D).

Comparison of the Permeabilities of the Neutral Forms of a Weak Base and a Weak Acid

We choose a weak acid AH/A^- whose $pK_a = {}^apK_a < 5$ so that at $pH_o \in [6; 8]$ its total concentration $C_a = [AH]_o + [A^-]_o \approx [A^-]_o$. We choose a weak base BH^+/B whose $pK_a = {}^bpK_a > 9$ so that at $pH_o \in [6; 8]$ its total concentration $C_b = [BH^+]_o + [B]_o \approx [BH^+]_o$. We set $C_a = C_b$ and find the pH_o ($\in [6; 8]$) for which the initial inward transmembrane flux of B ($F_B = P_B \times [B]_o$) is equal to that of AH ($F_{AH} = P_{AH} \times [AH]_o$):

$$F_B = F_{AH} \Leftrightarrow [AH]_o = (P_B/P_{AH}) \times [B]_o$$

$$\Leftrightarrow [H^+]_o/{}^aK_a \approx (P_B/P_{AH}) \times {}^bK_a/[H^+]_o$$

$$\Leftrightarrow pH_o \approx 0.5 \times ({}^apK_a + {}^bpK_a) - 0.5 \times \log(P_B/P_{AH}). \quad (5)$$

For $pH_i \in [6; 8]$, the initial rate of pH_i change induced by the weak acid is $-F_{AH}/\beta_i$ since, in the cell, most of AH dissociates to form $A^- + H^+$; similarly, the initial rate of pH_i change induced by the weak base is F_B/β_i. Thus, if one of the permeabilities is known, the other permeability can be deduced from the value of pH_o for which the initial direction of the pH_i change during the application of the mixture of the weak base and the weak acid reverses ($F_B = F_{AH}$).

Online Supplemental Material

The arguments leading from the observed changes in pH_i to the properties of the transporter molecule involve a model of transmembrane fluxes in the cell (essentially that used by Marcaggi et al., 1999) and a multistate model of a hypothetical NH_4^+-Cl^- cotransporter with K^+ inhibition. Details of these models and their analysis are available online at http://www.jgp.org/cgi/content/full/116/2/125/DC1

RESULTS

In agreement with Marcaggi et al. (1999), pH_i in bundles of glial cells superfused with solution at the physiological pH of 6.90 had values up to ~7.55 (e.g., see Fig. 7). More acid pH_is (<7.0) were encountered in bundles that were visibly damaged or whose pH_i recovered only slowly from an acid load. In slices of bee retina, mean pH_i measured in glial cells selected for their negative membrane potentials has been reported as 7.31 (Coles et al., 1996). For this reason, and also because the amplitude of pH_i responses of isolated bundles to NH_4^+ application correlated positively with pH_i (Marcaggi et al., 1999), bundles with $pH_i > 7.1$ were usually selected, except for some experiments on NH_3 permeability for which a more acid baseline pH_i was advantageous (e.g., see Fig. 4).

The Ammonium-induced Decrease in pH_i Is Inhibited by a High Concentration of K^+_o

Fig. 2 A illustrates how 2 mM ammonium applied for 30 s to an isolated bundle of bee retinal glial cells at the measured physiological pH_o of 6.90 (Cardinaud et al., 1994) causes a decrease in pH_i, indicating entry of NH_4^+. Marcaggi et al. (1999) have reported that this acidification requires external Cl^- (but not Na^+) and is inhibited by bumetanide (at 100 μM) and by piretanide, properties of the family of K^+-Cl^- cotransporters. Between applications of NH_4^+ in Fig. 2 A, the external K^+ concentration ($[K^+]_o$) was at its normal physiological value of 10 mM (Cardinaud et al., 1994), and it was maintained at this value during the second and fifth applications of NH_4^+. For the first NH_4^+ application, $[K^+]_o$ was reduced to 1 mM, which slightly increased the acidification, and for the third application it was increased to 50 mM. Although increasing $[K^+]_o$ to 50 mM for up to 2 min in the absence of ammonium caused only negligible changes in pH_i ($n = 6$; not shown), 50 mM K^+_o reduced the ammonium-induced acidification to about half that in the presence of 10 mM K^+_o. Rb^+, an ion that can replace K^+ in many transport processes, produced a greater inhibition that we did not investigate further (fourth ammonium application). Hence, Fig. 2 A suggests that inward transport of NH_4^+ is inhibited by K^+_o and Rb^+_o (as would be expected if NH_4^+ and K^+ (and Rb^+) competed for the same transporting site, for example). More interestingly, the inhibition may be relatively weak: increasing $[K^+]_o$ from 10 to 50 mM only halved the pH_i response to 2 mM ammonium, suggesting that the transport may be selective for NH_4^+ over K^+. To quantify this selectivity from measurements of pH_i, it was necessary to have a scheme of the transmembrane fluxes of NH_4^+ and NH_3 and to determine parameters relating these fluxes to changes in pH_i.

Parameters to be Determined

Fig. 2 B shows a response to a longer (5 min) application of ammonium on an expanded time scale. This response can be divided into five phases that can be explained by the schemes of Fig. 2 C (see also Boron and De Weer, 1976; Marcaggi et al., 1999). Initially, pH_i increases because of the predominant effect of the rapid entry of NH_3, which combines with H^+ (Phase 1). Since the equilibrium of the reaction $NH_3 + H^+ \leftrightarrow NH_4^+$ is so far to the right at pH near 7, it is sufficient that the inward flux of NH_3 exceeds ~1% of the inward flux of NH_4^+. As the ratio $[NH_4^+]_i/NH_3]_i \propto [H^+]_i$, Phase 1 is expected to be greater for cells with acid pH_i. This was actually the case: Phase 1 was detected only for cells with baseline $pH_i < 7.2$. When the NH_3 concentrations approach equality on each side of the cell membrane, there is still an inward NH_4^+ gradient because $[H^+]_o > [H^+]_i$. Then the NH_3 flux becomes outward while NH_4^+ continues to enter the cells and release H^+ ions (Phase 2). A steady state is reached (Phase 3) when the production of H^+ ions equals their extrusion by pH regulatory processes. When extracellular ammonium is suddenly removed, intracellular ammonium exits the cell faster in the NH_3 form than in the NH_4^+ form, so NH_4^+ dissociates to form NH_3 and there is a rebound acidification (Phase 4), followed by a slower return to baseline as proton equivalents are pumped out of the cell (Phase 5).

Marcaggi et al. (1999) showed that a simple mathematical model based on Fig. 2 D could simulate the main features of the experimental records, but used parameters that were only roughly estimated. We have now made more precise measurements of the following parameters required by the model: the absolute values of baseline pH_i, the buffering power (β_i), the NH_3 permeability (P_{NH3}), the pH_i regulation rate (characterized by a time constant τ_{reg}), and the Cl^- concentration gradient that can help drive NH_4^+ into the cell.

Absolute Determination of pH_i During Application of NH_4^+

The precise value of $pH_o - pH_i$ in the presence of external ammonium (the plateau phase) is related to the force driving NH_4^+ across the membrane and is our main moti-

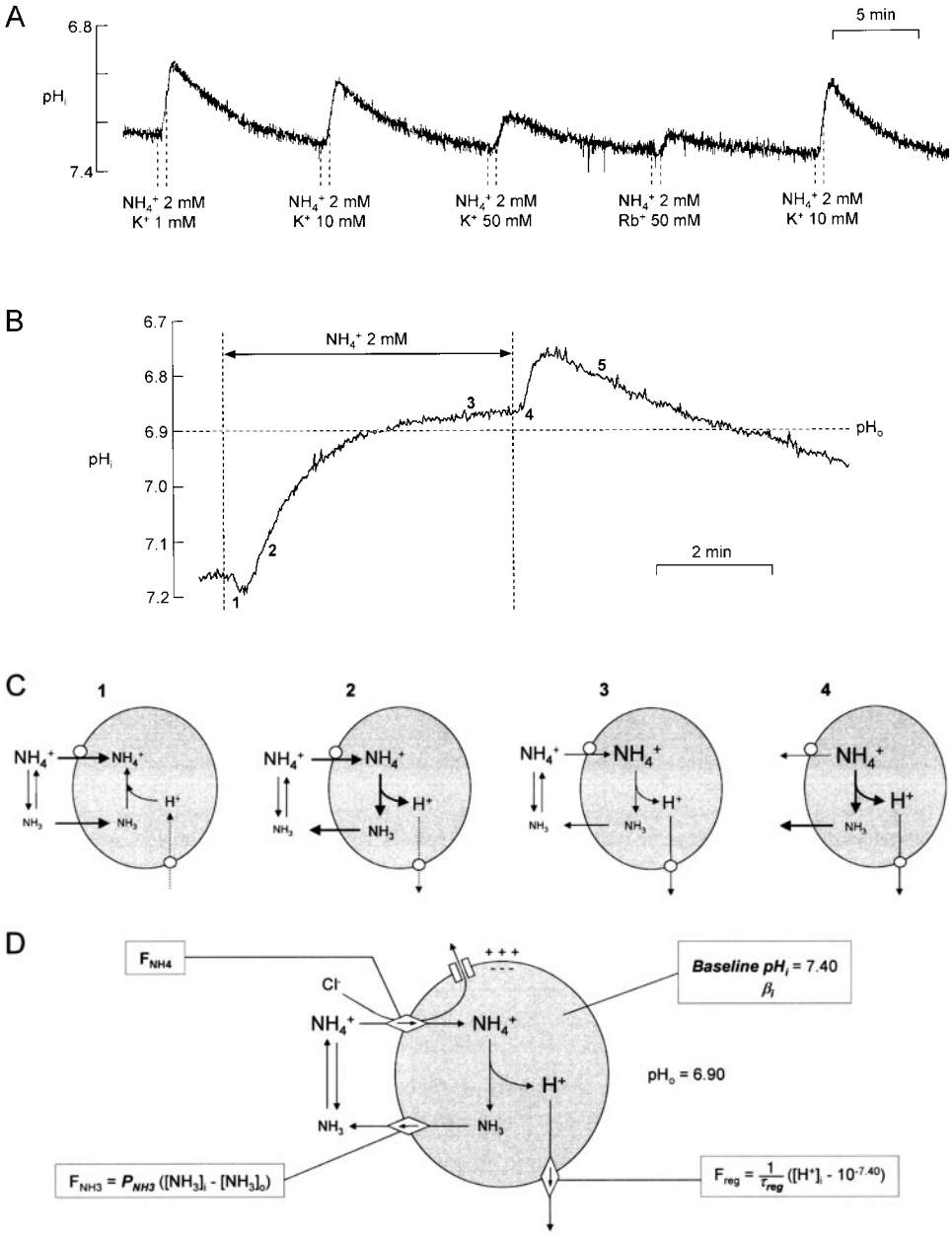

Figure 2. Effect of extracellular ammonium application on pH_i of an isolated bundle of glial cells. (A) The ammonium-induced acidification was slightly inhibited by K^+ or Rb^+. For each application of 2 mM NH_4^+, $[K^+]_o$ was either maintained at its baseline value of 10 mM, changed as indicated, or replaced by 50 mM Rb^+. (B) The response to a 5-min application of 2 mM NH_4^+ can be divided into five phases, which correspond to different patterns of fluxes (C). This cell had a fairly acid baseline pH_i (≈7.17) so that Phase 1 was prominent. (C) Schemes of fluxes corresponding to four of the phases indicated in B. (Phase 1) Inward flux of NH_3 is greater than ~1% of inward flux of NH_4^+. The maintenance of intracellular equilibrium $NH_4^+ \leftrightarrow NH_3 + H^+$ consumes H^+ ions. (Phase 2) NH_4^+ transmembrane gradient is still inward, while $[NH_3]_i$ slightly exceeds $[NH_3]_o$. H^+ ions are shuttled into the cell. (Phase 3) Extrusion of H^+ ions by pH regulatory mechanisms equals inward flux of NH_4^+. (Phase 4) This phase is approximately the inverse of Phase 1. Phase 5 (not shown) consists almost entirely of H^+ efflux. (D) Scheme of transmembrane fluxes during ammonium exposure. pH_i changes result from three transmembrane fluxes, F_{NH4}, F_{NH3}, and net H^+ flux through pH regulatory processes (F_{reg}) (see text).

vation for seeking an accurate measure of pH_i. Marcaggi et al. (1999) calibrated their measurements by applying nigericin, but it has been shown that this technique can give systematic errors (Nett and Deitmer, 1996; Boyarsky et al., 1996). To determine the absolute value of pH_i during NH_4^+ perfusion, we applied a weak acid and a weak base simultaneously as described by Eisner et al. (1989) (see materials and methods). Fig. 3 A shows a typical experiment. NH_4^+ was first applied at pH_o 6.90 and then at pH_o 7.30. At each plateau phase, ΔpH_i (10 mM propionate, 10 mM TMA) and ΔpH_i (10 mM propionate, 5 mM TMA) were in opposite directions, and we estimated by linear interpolation the concentration of TMA that would have given no change in pH_i when applied with 10 mM propionate (Eq. 4). The absolute value of pH_i was then calculated by Eq. 3. The method assumes that intracellular pK_a equals extracellular pK_a and that the membranes are relatively impermeable to the charged forms of the weak acid and base. This latter assumption was confirmed by the observation that, during applications of propionate (n = 21; not shown) or TMA (see Fig. 5 A), recovery of pH_i was slow and could be fully accounted for by pH regulatory processes. Since pH_i during the plateau phase depends partly on pH_i regulatory processes (Fig. 2 C 3), short NH_4^+ applications at the beginning and end of the experiment were made to check that the rates of recovery remained approximately the same. From 12 experiments, as in Fig. 3 A, pH_i was calculated to be 6.844 ± 0.017 (±SD, n = 12) after an 8-min application of NH_4^+ with pH_o = 6.90. This pH_i was significantly less than pH_o

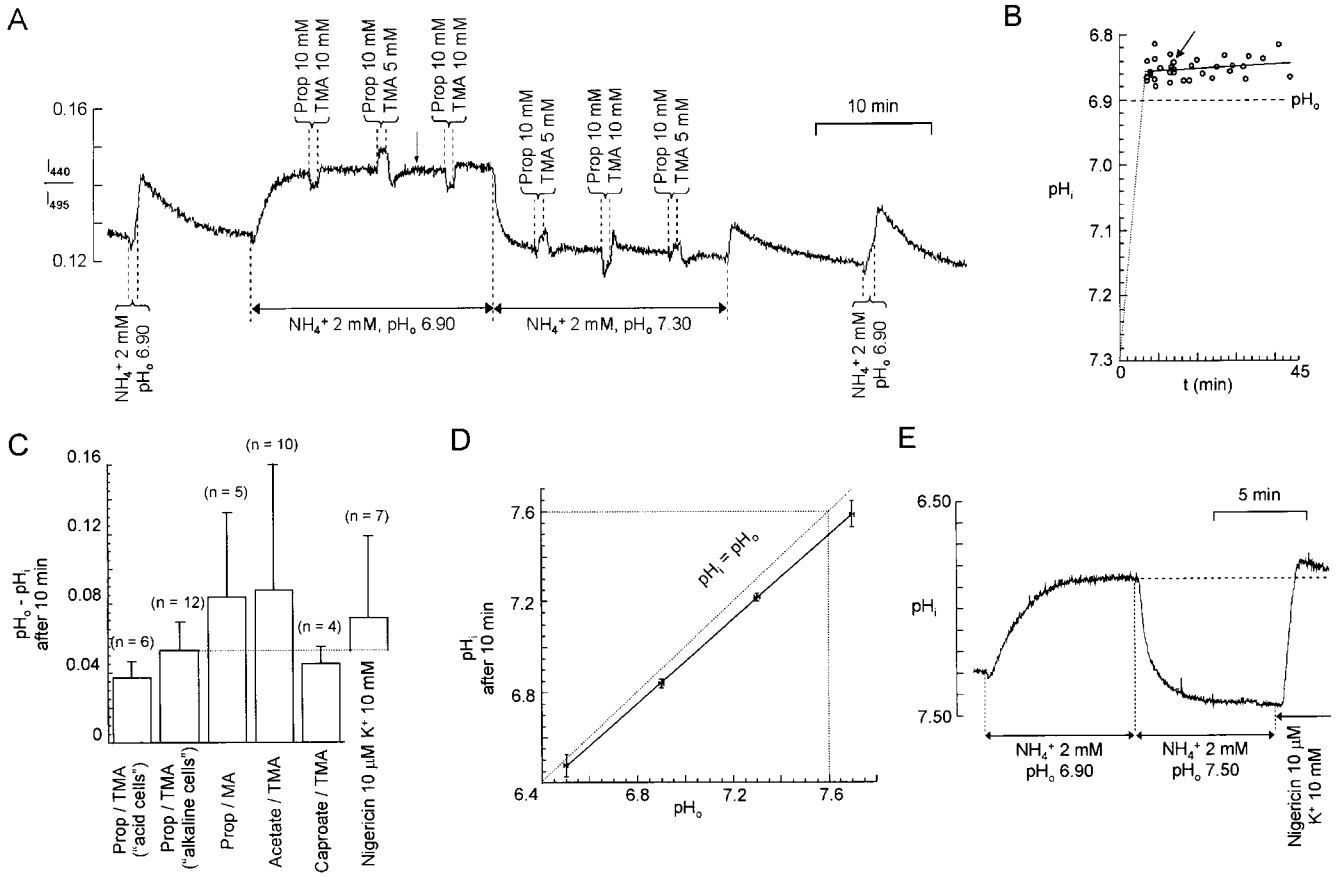

Figure 3. Absolute measurement of pH_i during application of 2 mM NH_4^+. (A) Recording of BCECF fluorescence ratio from a bundle of glial cells. Different mixtures of propionate (Prop) and trimethylamine (TMA) were applied during prolonged application of 2 mM ammonium, first with $pH_o = 6.90$, and then with $pH_o = 7.30$. (B) In experiments like that of A, pH_i was calculated from responses to application of two mixtures of propionate and TMA and ascribed to the time midway between the two applications (e.g., arrows in A and B correspond to the same point). The data points shown are for an ammonium concentration of 2 mM and the solid line is a linear regression through them. The dashed line simply illustrates that the mean initial pH_i was 7.3. (C) Summary of results for the pH_i measured ~10 min after application of 2 mM ammonium at pH 6.90. The results for different pairs of weak acids and weak bases are shown separately; for the pair propionate/TMA, a possible dependence on pH_i was examined by comparing the mean values for cells with an initial baseline $pH_i < 7.10$ ("acid") and those with baseline $pH_i > 7.10$ ("alkaline"). Bars show SDs. (D) Absolute pH_i reached during 2 mM NH_4^+ application at pH_os 6.50 ($n = 7$), 6.90 ($n = 6$), 7.30 ($n = 6$), and 7.70 ($n = 7$). The solid line is a linear regression through the data points (R = 0.996), vertical bars represent ±SD, horizontal bars represent the precision of the adjusted pH_o of the solutions. (E) Recording showing pH_i reached in nigericin 10 µM pH_o 6.90 compared with pH_i reached in NH_4^+ 2 mM pH_o 6.90.

($P < 0.0001$) and remained so for at least 35 min (Fig. 3 B). To see whether the result depended on the specific weak acid and weak base used, we used other weak acid/weak base couples. In experiments similar to that of Fig. 3 A, the estimated difference $pH_o - pH_i$ after >10 min of perfusion with 2 mM ammonium was not significantly different when the following couples were used: propionate/TMA; propionate/MA; acetate/TMA and caproate/TMA (Fig. 3 C). To see whether the value of ($pH_o - pH_i$) reached during the plateau phase was related to the baseline pH_i, we compared cells with a baseline $pH_i < 7.1$ with those with $pH_i > 7.1$ (Fig. 3 C, first two columns). The difference in the mean values of ($pH_o - pH_i$) during the plateau phase was not significant. In contrast, as illustrated in Fig. 3 A, the level of the plateau did indeed depend strongly on the pH_o at which the NH_4^+ was applied. Absolute values of pH_i estimated during superfusion with 2 mM NH_4^+ at pH_o 6.500 ± 0.005, 6.900 ± 0.005, 7.300 ± 0.005, and 7.700 ± 0.005 are plotted in Fig. 3 D and show a very precise linear correlation with pH_o such that ($pH_i - 6.142$) = 0.9264 × ($pH_o - 6.142$). In later experiments, we calibrated the measurements of pH_i simply by superfusing the cells with 2 mM ammonium for at least 8 min and using this relation.

Intracellular Buffering Power

The H^+ ions released into (or taken up from) the cytoplasm as a consequence of the transmembrane fluxes of NH_4^+ and NH_3 affect pH_i according to the relation

$\Delta pH_i = \Delta Q / \beta_i$, where ΔQ is the quantity of H^+ ions/U volume and β_i is the intracellular buffering power (see Roos and Boron, 1981). We estimated β_i by applying the weak acid propionate (as in Figure 1 of Marcaggi et al., 1996); the change in pH_i reached its maximum very rapidly compared with the time course of pH_i recovery in the presence of propionate, and we did not attempt to block pH_i regulation (compare Szatkowski and Thomas, 1989). Mean β_i was 12.2 ± 2.9 mM (n = 11) and we took 12 mM for the model.

To see if β_i varied markedly with pH_i, we shifted pH_i by applying NH_4^+ at various pH_os. The results and the analysis, which is complicated by the effects of the NH_3/NH_4^+ system, are given in Marcaggi (1999); the conclusion is that β_i is effectively constant in the range 6.7–7.3.

Permeability to NH_3

We estimated NH_3 permeability (P_{NH3}) from measurements of pH_i under conditions in which entry of NH_4^+ was blocked so that changes in pH_i were due only to the inward flux of NH_3. We have previously shown that NH_4^+ does not enter through barium-sensitive K^+ channels, the major cationic conductance in these cells, and also that NH_4^+ entry is totally blocked by bumetanide or by removal of external chloride (Marcaggi et al., 1999). We therefore applied ammonium in Cl^--free solutions to which, in some cases, bumetanide had been added, and measured the rate of change of pH_i (in the alkaline direction) induced by NH_3 entry into the cells.

With the cell bundles adhering to the floor of the perfusion chamber, we failed to find a molecule causing a 10–90% pH_i change faster than the one produced by ammonium: perhaps the change of solution at the cell membrane (0–20 μm from the floor of the chamber) was not fast enough for this measurement. To expose cells to faster solution changes, we caught hold of bundles of cells with a 3-μm tip diameter pipette and carried them 50–100 μm up from the floor of the chamber. To increase the time resolution of the rapid initial slope of the pH change, we measured the fluorescence ratio with faster switching of the excitation wavelengths (>3 Hz). To reduce delays due to diffusion, we applied ammonium at a high concentration (10 mM) but at an acid pH (6.50) so that $[NH_3]_o$ was low but benefited from facilitated diffusion (Engasser and Horvath, 1974). To increase the NH_3-induced ΔpH_i, baseline pH_i was reduced (to ~6.80) by perfusing the cells for 30–60 min with solution buffered at pH_o 6.20. After a 1-min perfusion with 0 Cl^- + 0.5 mM bumetanide, 10 mM ammonium was applied at pH_o 6.50 (Fig. 4 A). In these conditions, the 10–90%–pH_i change induced by 10 mM propionate (Fig. 4 B) was twice as fast as the one induced by ammonium, showing that the speed of solution change at the cell membrane did not significantly limit the influx of NH_3.

Although pH_i was ~7.00 during the ammonium application, while pH_o was 6.50, no slow pH_i decrease was observed, as would have been the case if the membranes had had some permeability to NH_4^+. This confirms that NH_4^+ pathways were insignificant in these conditions.

The slope of the pH_i change was measured at 50% of the ΔpH_i response, where it is known that $[NH_3]_o$ has reached its final concentration, since the effect of propionate is 90% at this time (Fig. 4). Since, for $pH_i \sim 7.00$, $[NH_4^+]_i > 100 \times [NH_3]_i$, then $\beta_i \times \delta pH_i/\delta t = \delta [NH_4^+]_i/\delta t \approx \delta ([NH_4^+]_i + [NH_3]_i)/\delta t = F_{NH3} \times {}^S/_V$, where F_{NH3} is the NH_3 transmembrane flux and ${}^S/_V$ is the ratio of membrane surface to intracellular volume in which the ammonium is distributed. The ratio of the surface to the total cell volume has been estimated to be ≈1.2 μm^{-1} (Marcaggi et al., 1999), but the ammonium will be present almost entirely in the water phase that occupies 0.775 of the total volume of the tissue (Coles and Rick, 1985). Taking this factor for the water content of the glial cells gives an estimated effective ${}^S/_V$ of 1.55 μm^{-1}. Knowing β_i, we could then calculate the transmembrane flux of NH_3 from the rate of change of pH_i: $F_{NH3} \approx {}^V/_S \times \beta_i \times \delta pH_i/\delta t$. From this flux, we found P_{NH3} = 14.7 ± 2.9 μm · s^{-1} (n = 6) in 0 Cl^- + 0.5 mM bumetanide, which was not significantly different from the value in 0 Cl^- only (n = 5), showing that bumetanide did not further inhibit NH_4^+ entry.

Holding up the cells with a pipette will have introduced some stress in the cell membrane, which may have modified its permeability. To check that NH_3 permeability is the same for cells plated on the bottom of the chamber (the conditions used for the other experiments), we also determined P_{NH3} by an indirect method. Methylamine (MA; $CH_3NH_3^+/CH_3NH_2$) is a weak base with a pK_a that is high (≈10.6; Robinson and Stokes, 1959) compared with that of ammonium (≈9.2). Because of this pK_a difference, at pH < 8 (at which charged forms are preponderant), if $[CH_3NH_3^+] + [CH_3NH_2] = [NH_4^+] + [NH_3]$, then $[CH_3NH_2] < 0.04 \times [NH_3]$. It follows that if P_{CH3NH2} (P_{MA}) is not far different from P_{NH3}, for equal concentrations of MA and ammonium applied, $F_{CH3NH2} << F_{NH3}$. This is why P_{MA} can be measured directly even with a slow speed of solution change at the cell membrane. Fig. 5 A illustrates the pH_i response to 10 mM MA compared with the pH_i response to 10 mM TMA ($pK_a \approx 9.6$). The speed of the pH_i change induced by TMA was far faster than the one induced by MA, showing that the speed of the solution change was fast enough for measurement of P_{MA}, which was found to be 27.4 ± 8.1 μm s^{-1} (n = 8). Once this permeability was known, it was possible to deduce the permeability of propionate by ascertaining

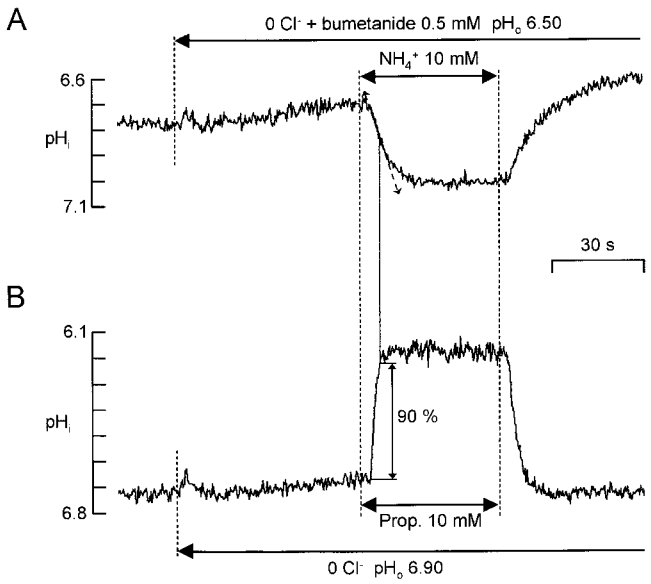

Figure 4. Direct measurement of P_{NH3}. (A) A bundle of cells was held with a pipette ~50 μm above the floor of the chamber and perifused for 30 min in pH_o 6.20 to reduce pH_i. The cells were then perifused with 0 Cl^- solution containing bumetanide 500 μM for 1 min before 10 mM $NH_4^+{}_o$ was substituted for $Na^+{}_o$. (B) A few minutes after the response of A, the same bundle attached to the pipette was perifused with 10 mM propionate in the same conditions. The propionate-induced pH_i change gave a lower limit for the speed of the change in solution at the cell membrane.

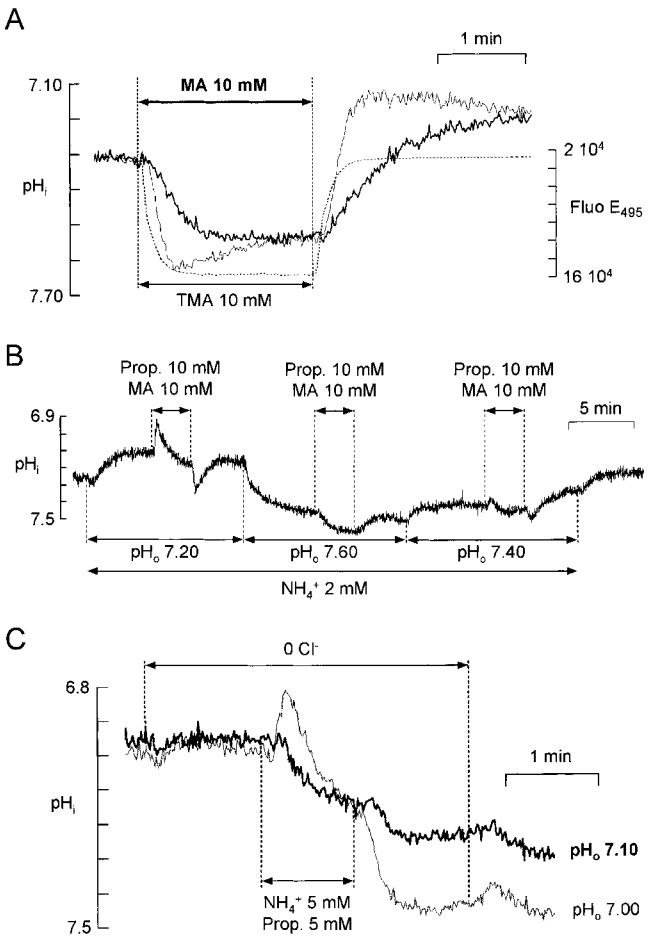

Figure 5. Indirect measurement of NH_3 permeability. (A) Direct measurement of P_{MA}. The pH_i change induced by 10 mM methylamine (MA) (thick line) was compared with that induced by 10 mM trimethylamine (TMA) (thin line) and to the change in fluorescence on switching to a solution containing 1 μg $liter^{-1}$ fluorescein (dotted line). The microscope was focused on the same bundle for the three recordings. (B) Relative cell membrane permeabilities to neutral forms of propionate (Prop) and MA. A bundle of cells was superfused with 2 mM NH_4^+ so that pH_i was maintained at a value close to pH_o (Fig. 3 D). When 10 mM Prop + 10 mM MA was applied at pH_o 7.2, entry of the neutral form of Prop initially predominated, but as $[Prop]_i$ increased, entry of MA began to predominate and pH_i started to increase. The initial change in pH_i reversed for a value of pH_o between 7.40 and 7.60. (C) Relative cell membrane permeabilities to NH_3 and to the neutral form of Prop. A mixture of 5 mM NH_4^+ and 5 mM Prop was applied to cells superfused with a 0 Cl^- solution at pH_o 7.10 (thick trace) or 7.00 (thin trace). The two recordings were from the same bundle of cells. At pH_o 7.10, the initial change in pH_i was an increase, while at pH_o 7.00 it was a decrease.

the initial direction of the pH_i change induced by a simultaneous application of 10 mM propionate and 10 mM MA. To avoid too great a variation of the net ΔpH_i during this simultaneous application, we used a condition in which $pH_i \approx pH_o$, which was obtained by including 2 mM ammonium in the superfusate (Fig. 3 D). As illustrated in Fig. 5 B, the initial direction of the pH_i change reversed for $7.40 < pH_o < 7.60$ ($n = 4$). Taking the mean of this range ($pH_o \approx 7.50 \pm 0.10$) gives $x = P_{MA}/P_{prop} \approx 3.16 \pm 1.46$ according to Eq. 5. So, $P_{prop} = P_{MA}/x \approx 8.67 \pm 6.57$ μm s^{-1}.

The same protocol was used to estimate P_{NH3} from the now known P_{prop}, the simultaneous application being done in 0 Cl^- to prevent the entry of NH_4^+. As illustrated in Fig. 5 C, the initial direction of the pH_i change reversed for $7.00 < pH_o < 7.10$ ($n = 4$), which gives $x = P_{NH3}/P_{prop} \approx 1.02 \pm 0.24$ according to Eq. 5. So $P_{NH3} = x \times P_{prop} \approx 8.84 \pm 8.78$ μm s^{-1}.

In conclusion, the two methods of estimation of P_{NH3} gave values not significantly different. The standard deviation obtained with the second method was increased by the successive approximations so we give more weight to the value obtained with the first method and conclude that P_{NH3} is in the range of 7–19 μm s^{-1}; we take the value 13 μm s^{-1} for the model.

pH Regulation

When pH_i falls below its baseline value, pH regulatory mechanisms tend to restore it by extruding H^+ ions. To quantify the kinetics of this regulation, we acid loaded the cells by exposure to ammonium and analyzed the recovery (Roos and Boron, 1981; Thomas, 1984). Fig. 6

A shows the recoveries of pH_i in a single bundle of cells after initial displacements of various amplitudes induced by applications of ammonium at various concentrations. For each ammonium application, the recovery was analyzed for 8 min starting 45 s after the end of the application («t_f») to allow for the rebound acidification (Phase 4). The plot is semilogarithmic, the ordinate being $\ln([H^+]_i - [H^+]_\infty)$, where $[H^+]_\infty$ was the baseline $[H^+]_i$ at rest. Linear regressions showed that the recoveries were exponential irrespective of the initial displacement, and had slopes ($= -1/\tau_{reg}$) that were not systematically different.

Values of the time constant τ_{reg} for 17 bundles of cells for which at least three different ammonium concentrations were tested were plotted as a function of the initial pH_i displacement, $\Delta pH_i(NH_4^+)$ (Fig. 6 B). Linear regression of $\tau_{reg}[\Delta pH_i(NH_4^+)]$ confirmed that τ_{reg} was independent of the pH [mean slope of 0.3 ± 1.8 min (pH unit)$^{-1}$; $n = 17$]. We conclude that despite considerable variability, τ_{reg} was approximately constant irrespective of the initial pH_i displacement with a mean value of 3.0 ± 1.1 min ($n = 17$). We therefore described the pH_i regulation by Eq. 6:

$$F_{reg} = (1/\tau_{reg}) \times ([H^+]_i - [H^+]_\infty), \qquad (6)$$

with $\tau_{reg} = 3$ min.

Driving Force

The flux rate of a Cl^- cotransporter will depend in part on $[Cl^-]_o$ and $[Cl^-]_i$, and we will use values of these concentrations in the transporter model of Fig. 10 A (see online supplemental material). $[Cl^-]_o$ being known, we attempted to estimate $[Cl^-]_i$. Measurements in slices of bee retina with ion-selective microelectrodes have shown that in the glial cells Cl^- (and also K^+) are at close to electrochemical equilibrium (Coles et al., 1986, 1989). Hence, $[Cl^-]_i/[Cl^-]_o$ could be deduced approximately from V_m. We did not succeed in measuring V_m in the isolated bundles of glial cells directly (by electrode techniques) and used an indirect method. We argued that if the membranes were made permeable to H^+ then $[H^+]_i$ would be determined by V_m. We applied the H^+/K^+ exchanger, nigericin, in solutions with normal $[K^+]_o$ and observed the resulting change in pH_i (Fig. 3 E). The minimum pH_i reached during nigericin was compared with pH_i at the plateau phase induced by 2 mM NH_4^+, the mean difference being 0.02 ± 0.05 ($n = 7$; Fig. 3 C). It follows that the mean value of $pH_o - pH_i$ at the maximum of the nigericin-induced pH_i change was ~0.07 (Fig. 3 C). On the assumption that H^+, being now in equilibrium with K^+, was distributed passively across the membrane, V_m was −4 mV. Since nigericin is not perfectly selective for H^+ (Pressman et al., 1967; Margolis et al., 1989), it probably depolarized the membranes somewhat, as suggested by the slow increase in pH_i during nigericin (Fig. 3 E). Thus, the true V_m is probably more negative than −4 mV and $[Cl^-]_o/[Cl^-]_i = \exp(-V_m F/RT) > 1.18$.

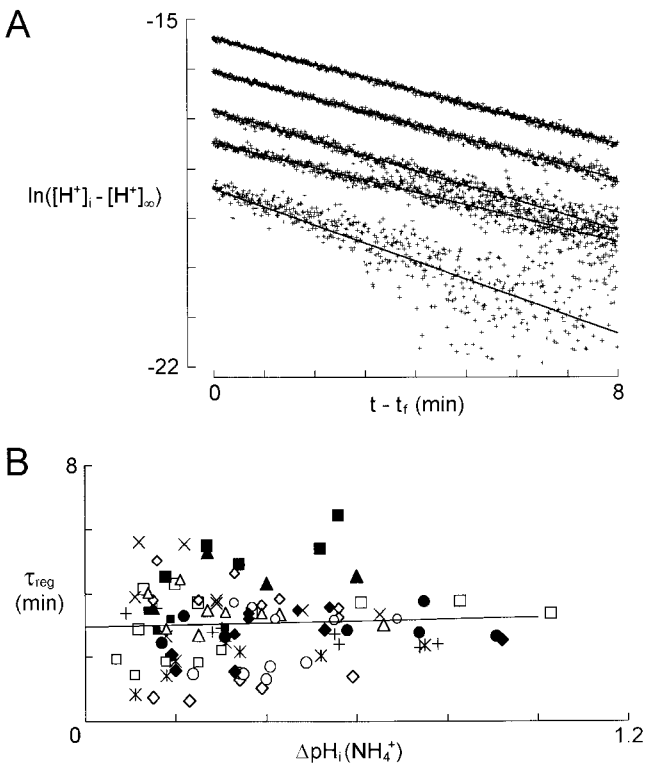

Figure 6. pH_i recovery from ammonium-induced acid loads. (A) Analysis of recoveries from acidifications induced by applications of 0.5, 1, 2, 5, and 10 mM NH_4^+ on the same bundle of glial cells. $\ln([H^+]_i - [H^+]_\infty)$ was plotted against $t - t_f$, where t_f is 45 s after the end of the NH_4^+ superfusion. From linear regressions of the data points, τ_{reg} was calculated as being (min): 2.74 (correlation coefficient, R = 0.761), 3.96 (R = 0.971), 3.29 (R = 0.978), 3.68 (R = 0.996), and 3.75 (R = 0.998) for the recoveries from the increasing acidifications induced by 0.5, 1, 2, 5, and 10 mM NH_4^+. (B) τ_{reg}, calculated as in A, as a function of ΔpH_i at the beginning of the recovery. The data are from 17 cell bundles (each represented by a different symbol) for which at least three different $[NH_4^+]_o$ were applied. For each cell bundle, a linear regression was calculated and a line with the mean of their slopes [(0.3 min (pH unit)$^{-1}$] is shown passing through the barycenter of the points.

Concentration Dependence of the pH_i Changes Induced by 30-s Applications of Ammonium

To record the responses to increasing concentrations of NH_4^+ in the absence of external K^+, we superfused the cells in 0 K^+ for 15 s before and during each NH_4^+ application (Fig. 7 A). Repeated exposure to high $[NH_4^+]$ appeared to lead to impairment of pH_i regulation and, for 7 of 11 experiments, pH_i did not recover from the acidification induced by 10 mM NH_4^+. Measurements were therefore made only on the records from the four experiments for which pH_i recovered

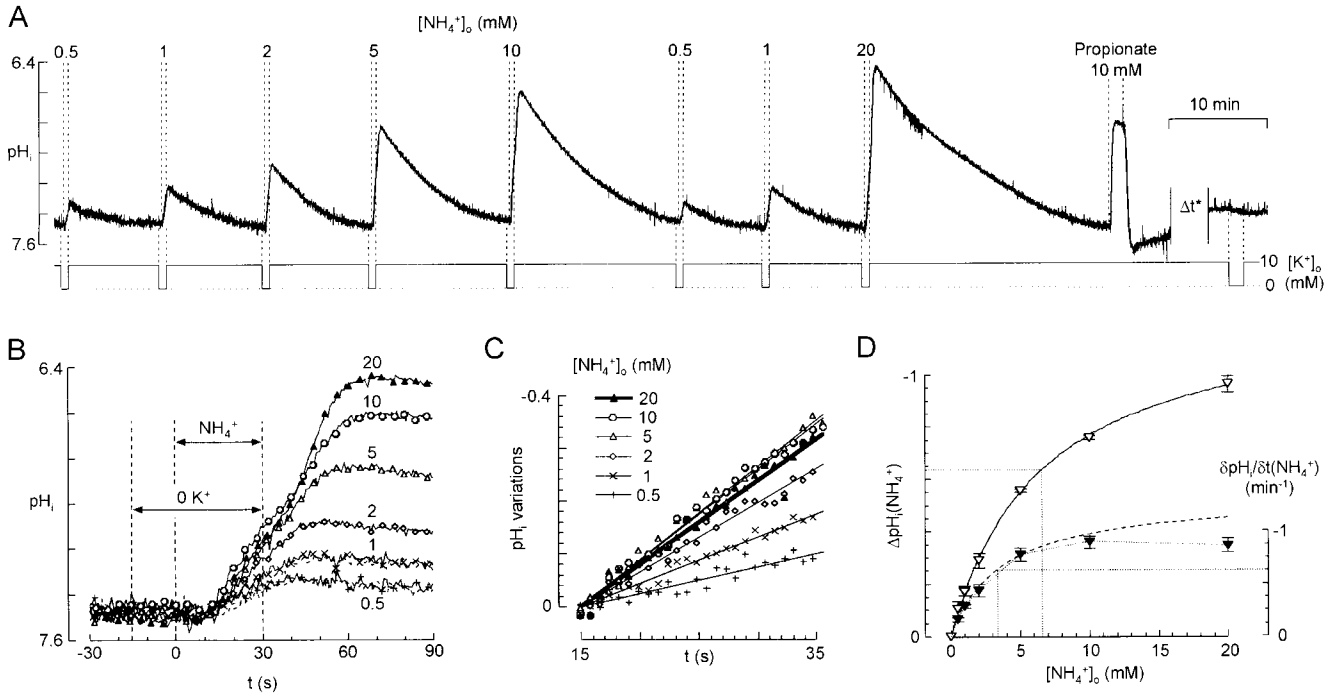

Figure 7. pH_i changes as a function of ammonium concentration (for 30-s applications in 0 K^+). (A) Typical recording of pH_i responses to various NH_4^+ concentrations. Cells were normally superfused with 10 mM K^+ standard solution that was switched to a 0 K^+ solution 15 s before each NH_4^+ application. The response to 10 mM propionate (near the end of the experiment) gives a lower limit for the rapidity of the solution changes. On the same cells, after a delay of ≈20 min ("Δt*"), removal of extracellular K^+ with no ammonium application had no detectable effect on pH_i. (B) Superposition of pH_i responses to NH_4^+ (from A) on a shorter time scale. Dotted lines for 0.5 and 1 mM NH_4^+ are the second (control) responses. The delay between activation of the solenoid valve ($t = 0$) and the start of the changes in pH_i was ~10 s. Note that during the NH_4^+ application, pH_i fell more rapidly for 10 mM NH_4^+ than for 20 mM, but that the peak reached after the application (Phase 4) was greater for 20 mM. (C) Calculation of $\delta pH_i/\delta t(NH_4^+)$ for each NH_4^+-induced acidification. Mean slopes were measured between 15 and 35 s after the onset of the NH_4^+ application by linear regression. Taking into account the delay for arrival of solutions, this interval corresponds to the last 20 s of the NH_4^+ applications. (D) Mean values for $\Delta pH_i([NH_4^+]_o)$ (peak change in pH_i, open symbols) and $\delta pH_i/\delta t([NH_4^+]_o)$ (filled symbols) from four experiments similar to that of A. Bars represent ± SEM. The best Michaelis-Menten fits of $\Delta pH_i([NH_4^+]_o)$ for $[NH_4^+]_o$ = 0.5, 1, 2, 5, 10, and 20 mM (solid line) and of $\delta pH_i/\delta t([NH_4^+]_o)$ for $[NH_4^+]_o$ = 0.5, 1, 2, and 5 mM (dotted line) are shown.

from 10 mM NH_4^+ and for which the response to subsequent control application of 0.5 or 1 mM NH_4^+ was closely similar to the initial response (in the record of Fig. 7 A, a final application of 20 mM NH_4^+ was made). To make sure that the effect of NH_4^+ was not rate limited by the speed of the solution change (as was probably the case in the previous study by Marcaggi et al., 1999), we checked that application of propionate gave a more rapid pH_i change (Fig. 7 A). Data were analyzed only for experiments in which the time for the 10–90% propionate-induced pH_i change was <15 s. The last part of Fig. 7 A shows that 0 K^+ alone did not affect pH_i on the time and pH scales of these experiments.

Fig. 7 B shows the NH_4^+ responses from the record of Fig. 7 A on a shorter time scale. The time of onset of the response to propionate (not shown) indicated that in this experiment there was a dead time of ~5 s between the switching of the electromagnetic valves and the arrival of a new solution at the cell membrane. The slope of the NH_4^+-induced pH_i change ($\delta pH_i/\delta t$) was measured before the rebound (Phase 4), between 15 and 35 s after the valves were actuated. $\delta pH_i/\delta t(NH_4^+)$ was calculated by linear regression as shown in Fig. 7 C. $\delta pH_i/\delta t(NH_4^+)$ increased with $[NH_4^+]_o$ in the range 0.5–10 mM NH_4^+; but for 20 mM NH_4^+, although the total pH_i change induced by NH_4^+ [$\Delta pH_i(NH_4^+)$] continued in every case to increase, in three of the four experiments, $\delta pH_i/\delta t$ for 20 mM NH_4^+ was less than for 10 mM, as in the example shown in Fig. 7, A–C. Mean data from the four experiments are shown in Fig. 7 D. $\Delta pH_i([NH_4^+]_o)$ was well fitted by a Michaelis-Menten curve $\Delta pH_i([NH_4^+]_o) = a[NH_4^+]_o/(b + [NH_4^+]_o)$ ($R = 0.993$) with half saturation, b, for $[NH_4^+]_o = 6.62 \pm 0.57$ mM ($n = 4$). But $\delta pH_i/\delta t([NH_4^+]_o)$ could only be fitted by a Michaelis-Menten curve for $[NH_4^+] \leq 5$ mM ($R = 0.926$), half saturation being at $[NH_4^+]_o = 3.37 \pm 0.98$ mM ($n = 6$) (Fig. 7 D). Because the relation between NH_4^+ transport and pH_i changes is indirect, the value of $[NH_4^+]_o$ that half saturates pH_i changes does not necessarily correspond to the one that half saturates transport of NH_4^+. To deduce the flux of NH_4^+, we had recourse to a mathematical model.

Dependence of NH_4^+ Flux on $[NH_4^+]_o$

Three transmembrane fluxes determine pH_i during and after application of ammonium (Fig. 2 C). Of these, we have a phenomenological description of the pH_i regulation (F_{reg} in Fig. 2 D), and we assume that the flux of NH_3 (F_{NH3} in Fig. 2 D) results from simple diffusion (Fick's law). To deduce the flux of NH_4^+ through the cotransporter (F_{NH4} in Fig. 2 D) from the changes in pH_i, we use the model of Fig. 2 D, expressed mathematically in the supplemental material. From the measurements described above, values for parameters of the model were: $\beta_i = 12$ mM, $pH_i = 7.4$, $\tau_{reg} = 3$ min, and $P_{NH3} = 13\ \mu m\ s^{-1}$. The surface-to-volume ratio, $^S/_V$, with its attendant uncertainty, was used to calculate P_{NH3}, but cancels out in the calculations.

As a first step, a constant inward F_{NH4} ($^{in}F_{NH4}$) was imposed for 30 s, with $[NH_4^+]_o$ (+ $[NH_3]_o$) set to 2 mM. The resulting $\delta pH_i/\delta t$ was calculated 15 s after the onset of the imposed $^{in}F_{NH4}$ and plotted against $^{in}F_{NH4}$ for various P_{NH3} (7, 13, and 19 $\mu m\ s^{-1}$; Fig. 8 A). Increasing P_{NH3} increased $\delta pH_i/\delta t$, but only slightly, showing that P_{NH3} is not a major rate-limiting factor.

A similar simulation, still using an imposed $^{in}F_{NH4}$, was then performed in the presence of various $[NH_4^+]_o$ (+ $[NH_3]_o$). Increasing $[NH_4^+]_o$ increased $[NH_3]_o$, reduced outward F_{NH3}, and, as expected, reduced $\delta pH_i/\delta t(^{in}F_{NH4})$ (Fig. 8 B). It is clear that the experimental result in which $\delta pH_i/\delta t$ was smaller for an application of 20 mM ammonium than for 10 mM (Fig. 7) does not necessarily imply that inward F_{NH4}(20 mM NH_4^+) < inward F_{NH4}(10 mM NH_4^+). We also note that since the relation of $\delta pH_i/\delta t$ to $^{in}F_{NH4}$ is curved (Fig. 8, A and B), $\delta pH_i/\delta t$ vs. $[NH_4^+]_o$ will saturate more rapidly than will $^{in}F_{NH4}$ vs. $[NH_4^+]_o$.

The pH_i peak reached after withdrawal of external ammonium must depend both on $[NH_4^+]_i$ at the end of the ammonium application, and on the effluxes of NH_4^+ and of NH_3 after withdrawal. To start modeling this, we considered the case of a 30-s application of 2 mM extracellular NH_4^+ with a constant $^{in}F_{NH4}$ (6.65 mM min^{-1} in Fig. 8 C). After removal of extracellular NH_4^+, the concentration gradient of NH_4^+ is outwards. We tested the simplest reasonable assumption, which is that outward $F_{NH4} = {}^{out}F_{NH4} \propto [NH_4^+]_i$. With no loss of generality, this can be written: $^{out}F_{NH4} = {}^{out}F_{NH4\ max} \times ([NH_4^+]_i/[NH_4^+]_{i\ max})$, where $[NH_4^+]_{i\ max}$ is the intracellular NH_4^+ concentration reached at $t = 30$ s and $^{out}F_{NH4\ max}$ is an initially arbitrary constant corresponding to the maximum transient $^{out}F_{NH4}$. As illustrated in Fig. 8 C, the rebound acidification on removal of extracellular NH_4^+ is maximal for zero $^{out}F_{NH4}$ and decreases with increasing $^{out}F_{NH4}$. Let $\Delta pH_i(^{in}F_{NH4})$ be the total pH_i change induced by a 30-s $^{in}F_{NH4}$ followed by an $^{out}F_{NH4}$ defined as above. From the experimental data, the mean ratio $\Delta pH_i/(\delta pH_i/\delta t)$ measured from 30-s applications of 2 mM NH_4^+ in 0 K^+_o was 0.60 ± 0.12 min ($n = 10$); the closest approach to this in

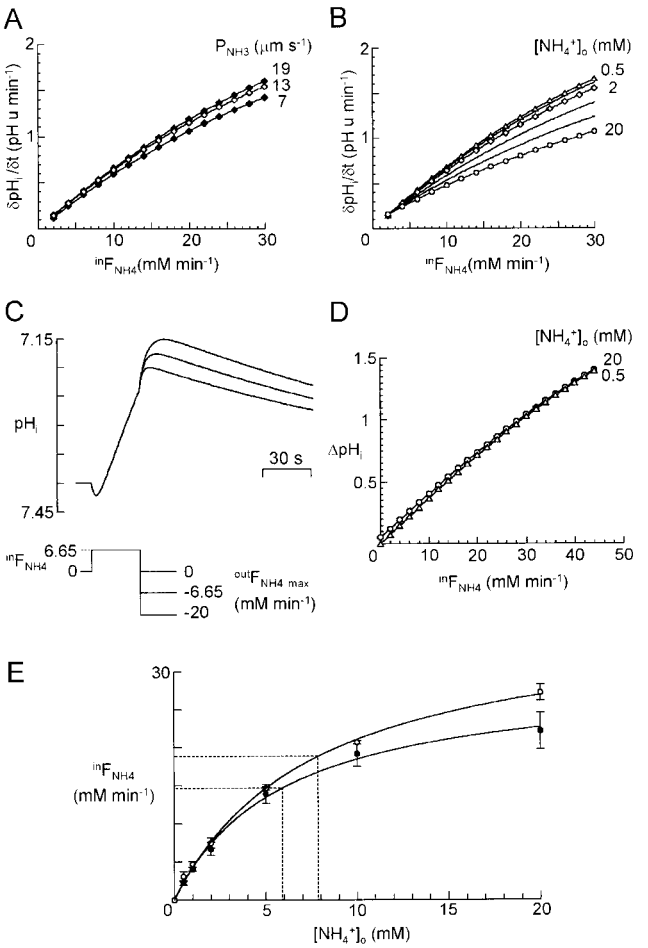

Figure 8. Use of the cell model (Fig. 2 D) to derive inward $F_{NH4}([NH_4^+]_o)$ from measured pH_i changes induced by brief applications of NH_4^+. (A) Constant inward F_{NH4} ($^{in}F_{NH4}$) was imposed on the model for 30 s. $\delta pH_i/\delta t$, calculated 15 s after onset, was plotted against $^{in}F_{NH4}$. Data are shown for simulations with $[NH_4^+]_o$ set to 2 mM (to fix $[NH_3]_o$) and $P_{NH3} = 7$, 13, and 19 $\mu m\ s^{-1}$. (B) As in A, $\delta pH_i/\delta t$ was plotted versus $^{in}F_{NH4}$ for simulations with $[NH_4^+]_o = 0.5$ mM (triangles), 1 and 2 mM (diamonds), and 5, 10, and 20 mM (circles). $P_{NH3} = 13\ \mu m\ s^{-1}$. Because increasing $[NH_4^+]_o$ increases $[NH_3]_o$, $\delta pH_i/\delta t(^{in}F_{NH4})$ is smaller for higher $[NH_4^+]_o$. (C) Simulations in which an $^{in}F_{NH4}$ was imposed for 30 s and followed by an outward F_{NH4} ($^{out}F_{NH4}$). $^{in}F_{NH4}$ was set to 6.65 mM min^{-1} and $[NH_3]_o$ was fixed by setting $[NH_4^+]_o = 2$ mM; this gave $\delta pH_i/\delta t = 0.44$ pH unit min^{-1}, equal to the mean measured pH_i change induced by 2 mM NH_4^+ in 0 K^+ for cells with baseline $pH_i \approx 7.4$. At $t = 30$ s, F_{NH4} switched instantaneously from $^{in}F_{NH4}$ to maximum $^{out}F_{NH4}$, $^{out}F_{NH4\ max}$, and decreased to zero as $[NH_4^+]_i$ decreased to zero (see text). Simulations for $^{out}F_{NH4\ max}$ equal to 0, −6.65, and −20 mM min^{-1} show that the rebound acidification after 30 s decreased when $^{out}F_{NH4\ max}$ increased. (D) Plot of $\Delta pH_i(^{in}F_{NH4})$ measured as baseline pH_i (7.4) minus the minimal pH_i reached during the rebound acidification after 30 s of influx $^{in}F_{NH4}$. Simulations for 0.5 mM (triangles) or 20 mM (circles) $NH_4^+{}_o$ ($+NH_{3o}$) show that $[NH_3]_o$ has little effect on $\Delta pH_i(^{in}F_{NH4})$. $^{out}F_{NH4\ max} = 0$. (E) $^{in}F_{NH4}([NH_4^+]_o)$ calculated from $\delta pH_i/\delta t([NH_4^+]_o)$ (●) and $\Delta pH_i([NH_4^+]_o)$ (○) of Fig. 7 D. The points were fitted by Michaelis-Menten curves (R = 0.963 and 0.994, respectively) with apparent constants K'_m equal to 5.9 ± 1.3 and 7.8 ± 0.7 mM.

Fig. 8 C is 0.56 min for ${}^{out}F_{NH4\,max} = 0$, which we accept as an approximation. $\Delta pH_i({}^{in}F_{NH4})$ is very little affected by $[NH_4^+]_o$ (still for an imposed ${}^{in}F_{NH4}$; Fig. 8 D), much less so than is $\delta pH_i/\delta t$ (Fig. 8 B). Thus, the inverse operation of estimating inward $F_{NH4}([NH_4^+]_o)$ is better done from $\Delta pH_i([NH_4^+]_o)$ than from $\delta pH_i/\delta t([NH_4^+]_o)$. By comparing experimental $\Delta pH_i([NH_4^+]_o)$ (Fig. 7 D) and simulated $\Delta pH_i({}^{in}F_{NH4})$ (Fig. 8 D), we calculated ${}^{in}F_{NH4}([NH_4^+]_o)$ (Fig. 8 E). The points were well fitted by a Michaelis-Menten equation of the form (Eq. 7):

$$ {}^{in}F_{NH4}([NH_4^+]_o) = {}^{in}F_{NH4max}\frac{[NH_4^+]_o}{K'_m + [NH_4^+]_o}. \quad (7) $$

The constant, K'_m, corresponding to half saturation of inward F_{NH4}, was 7.8 ± 0.7 mM. Variant analyses {from $\delta pH_i/\delta t([NH_4^+]_o$ or using Lineweaver-Burke plots} all gave lower values, down to 4.9 mM (Marcaggi, 1999). We conclude that $K'_m = 7.8$ mM is a conservative estimate of the affinity (an upper limit for K'_m) of the transporter for NH_4^+ in these experimental conditions.

Functional Selectivity for NH_4^+ over K^+

Having established the dependence of ${}^{in}F_{NH4}$ on $[NH_4^+]_o$ (for 30-s applications of ammonium), we then extended the approach to analyze the inhibitory effect of K^+. Fig. 9 A shows an experiment in which cells were superfused for 30 s with NH_4^+ in 0 or 10 mM K^+. $\Delta pH_i([NH_4^+])$ from six such experiments is shown plotted with double inverse scales as a function of $[NH_4^+]_o$ in Fig. 9 B. Using the model, as described above, a value of ${}^{in}F_{NH4}([NH_4^+])$ was deduced for each measurement of $\Delta pH_i([NH_4^+])$ and a second inverse plot was made (Fig. 9 C). This plot suggests that the inhibition was competitive since straight lines passing through the data points intersect near the ordinate axis (same ${}^{in}F_{NH4\,max}$).

Fig. 9 D illustrates how K^+ depolarizes these glial cells. In this record, from a glial cell in a retinal slice, the depolarization is greatly damped by electrical coupling between the cells and the slowness of the increase in $[K^+]$ in the extracellular clefts (Coles and Orkand, 1983). But in isolated cell bundles, the depolarization might be greater and in some way affect NH_4^+ uptake. We therefore used Ba^{2+}, which blocks the depolarization for at least 45 s after the application of K^+ (Fig. 9 D), to study the effect of K^+ on $\Delta pH_i(NH_4^+)$ in the absence of changes in membrane potential. In confirmation of Marcaggi et al. (1999), Ba^{2+} (at 5 mM) had in itself no effect on $\Delta pH_i(NH_4^+)$ ($n = 5$; not shown). Nor did it have a significant effect on the inhibition of $\Delta pH_i(NH_4^+)$ produced by raising K^+ to 20 mM (n =

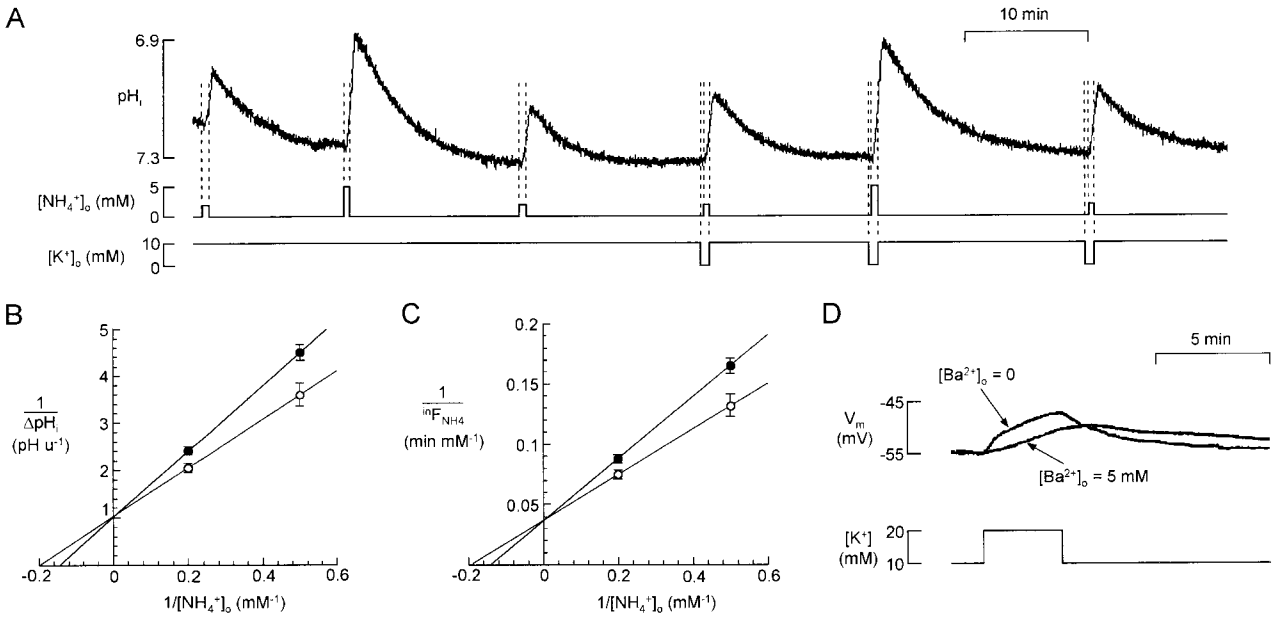

Figure 9. Inhibition of inward NH_4^+ flux by external K^+. (A) Comparison of responses to 2 and 5 mM NH_4^+ in 0 and 10 mM K^+. For each response, NH_4^+ was applied for 30 s; when applied in 0 K^+, K^+ was removed from the superfusate 15 s earlier. (B) Double inverse plot of mean ΔpH_i vs. $[NH_4^+]_o$ ($n = 6$). Straight lines passing through mean data points intersect the abscissa at $[NH_4^+]_o = 5.02$ mM (0 K^+, ○) and 6.90 mM (10 mM K^+, ●). (C) Double inverse plot of ${}^{in}F_{NH4}$ vs. $[NH_4^+]_o$. ${}^{in}F_{NH4}$ is the mean value during the NH_4^+ application calculated from ΔpH_i of the six experiments of B using the relation of Fig. 8 E. Straight lines passing through mean data points intersect the abscissa for $[NH_4^+]_o = 5.16$ mM (0 K^+, ○) and 7.09 mM (10 mM K^+, ●). (D) Intracellular recording from a retinal slice with a microelectrode in the glial compartment. Increasing $[K^+]$ from 10 to 20 mM in the superfusate induced a depolarization of the cell membranes. When the same increase of $[K^+]$ was made after superfusing the slice with 5 mM barium for a few minutes, the depolarization was undetectable for at least the first 45 s.

11; not shown). Hence, the depolarization is unlikely to be responsible for the inhibition of NH_4^+ transport by extracellular K^+.

To quantify the inhibitory effect of K^+, we calculated an apparent inhibitory constant, K'_i, defined by: $K''_m = K'_m\ (1 + [K^+]_o/K'_i)$, where K'_m is the Michaelis-Menten constant estimated above from responses to NH_4^+ in 0 K^+ and K''_m is the constant estimated from the responses to NH_4^+ in 10 mM K^+. K'_i was found to be 26.7 mM, which is greater than K'_m ($\leq$7.8 mM). Variant analyses also gave $K'_i > K'_m$ (see Marcaggi, 1999).

Affinities of the Transporter Molecule for NH_4^+ and K^+

In the previous two sections, we established the dependence of the mean inward F_{NH4} on $[NH_4^+]_o$ during 30-s (brief) applications of ammonium, and the inhibition of this flux by $[K^+]_o$. We now describe the changes in pH_i under more varied conditions; notably, longer applications of NH_4^+. These more complex responses impose additional constraints on the interpretation of the underlying processes and allow us to test whether the transport can be described by a standard minimal kinetic model of membrane cotransport to which we add competition by K^+ for the NH_4^+ binding site (Fig. 10 A). As explained by Sanders et al. (1984), the kinetic behavior of a cotransporter can be accounted for by models with different orders of binding of ions; we have chosen to consider binding first of Cl^- then K^+ or NH_4^+. This and other assumptions implicit in the model of Fig. 10 A, their justification where possible, and the techniques used to deduce the parameter values from experimental responses to NH_4^+ are given in the online supplemental material. Using the experimental results obtained so far, the model suggested that K_m, the binding affinity for NH_4^+, was 6–8 mM and K_i, the binding affinity for K^+, was in the range 10–20 mM, values that we now refine.

In the experiment of Fig. 10 B, $[NH_4^+]_o$ was increased in steps, each lasting 8 min. The level of the plateau phase (Phase 3 in Fig. 2 B) rose no further for $[NH_4^+]_o > 5$ mM ($n = 4$). Fig. 10 C shows simulated responses to the same protocol of stepwise increases in $[NH_4^+]_o$ for a cell containing the transporter model of A with $K_i = 15$ mM and $K_m = 5$ mM (continuous trace) or 20 mM (dashed trace). It is seen that the time course of pH_i, particularly for the step change $[NH_4^+]_o$ from 5 to 10 mM, is better simulated with $K_m = 5$ mM; i.e., with $K_m < K_i$.

Increasing $[K^+]_o$ in the Presence of NH_4^+

Fig. 11 A illustrates the inhibitory effect on NH_4^+ transport of increasing $[K^+]_o$ during the plateau phase induced by a long application of NH_4^+. An increase in $[K^+]_o$ from 10 to 50 mM rapidly increased pH_i by 0.092 $\pm$ 0.012 pH unit in 2 min in 2 mM NH_4^+ ($n = 5$) and

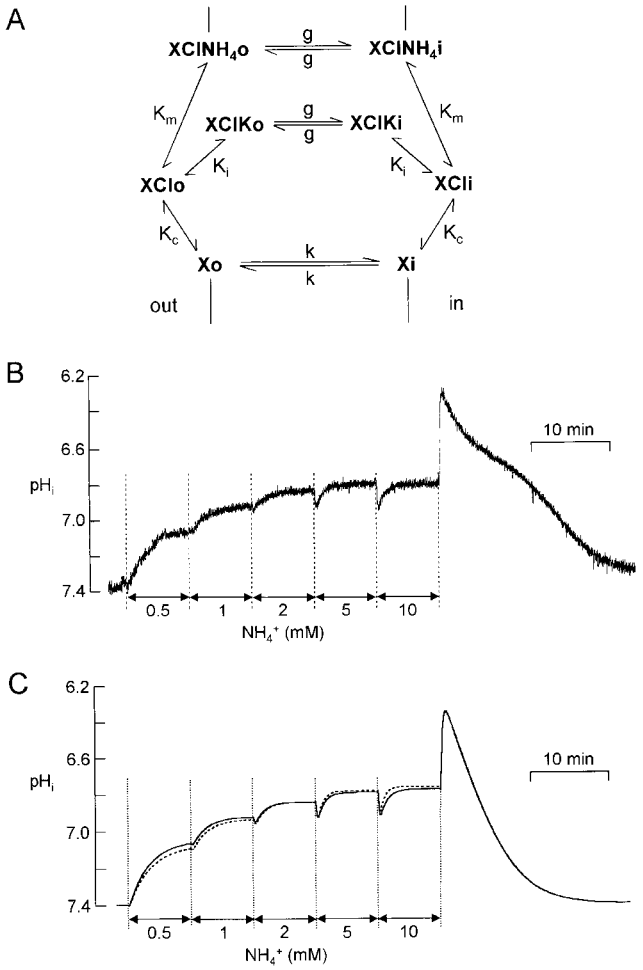

Figure 10. pH_i responses to stepwise increases in $[NH_4^+]_o$ are accounted for by a model of the transport process. (A) Kinetic scheme of the cotransport of Cl^- and NH_4^+ or K^+. The unloaded transporter molecule is symbolized by X; o or i indicate the position of the transporter at the external or internal side of the cell membrane. Binding ions Cl^-, NH_4^+, and K^+ are not shown in this scheme for visual simplicity. The three binding constants K_c, K_m, and K_i for Cl^-, NH_4^+, and K^+ are unaffected by the side to which the transporter faces. Two kinetic constants, k and g, describe the transit steps of the unloaded and loaded transporter. (B) Experimental response to stepwise increases in $[NH_4^+]_o$. (C) Simulated response of the cell model of Fig. 2 D including the transporter model of A to stepwise increases in $[NH_4^+]_o$ with affinity for NH_4^+, $K_m = 5$ mM (continuous line) and 20 mM (dashed line). K_i was 15 mM.

by a greater amount, 0.115 $\pm$ 0.022 pH unit in 20 mM NH_4^+ ($n = 5$). The difference is significant with $P = 0.01$. This observation raised the question of whether the inhibition by $[K^+]_o$ was purely competitive.

Simulations were performed with the transporter model of Fig. 10 A and the protocol of Fig. 11 A. K_m was set to 7 mM. Simulations with $K_i = 10$, 15, and 20 mM (Fig. 11 B) show that inhibition by a 2-min increase in $[K^+]_o$ from 10 to 50 mM differed from the experimental record in three aspects. First, the inhibition in 20

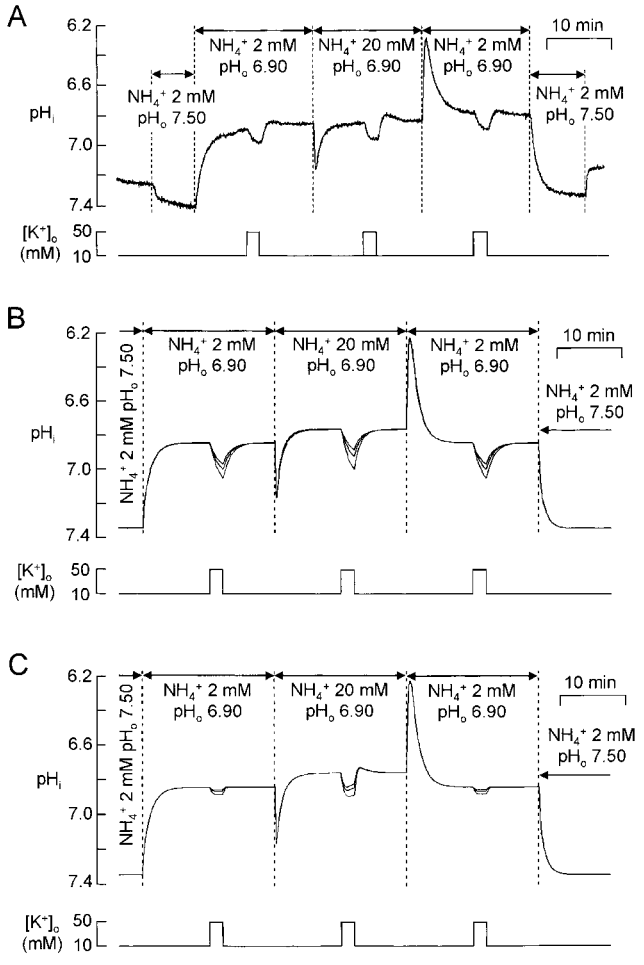

Figure 11. Effects of increasing $[K^+]_o$ from 10 to 50 mM on the plateau phase pH_i during superfusion with 2 mM or 20 mM NH_4^+. (A) Typical recording. At the beginning and end of the experiment, the cells were superfused with 2 mM NH_4^+ at pH_o 7.50 to provide a pH_i calibration (see Fig. 3 D). (B) Simulated effect of increasing $[K^+]_o$. In the model, $[K^+]_i$ was kept constant when $[K^+]_o$ was increased. The cell model included the transporter of Fig. 10 A (see online supplemental material for full list of parameter values). K_m was 7 mM and K_i was 10, 15, or 20 mM (superposed traces), the greatest inhibition being for K_i = 10 mM. (C) Simulation with the model modified so that transport of NH_4^+ was inhibited by extracellular K^+ in a noncompetitive manner. The transporter of Fig. 10 A was modified by removing the effect of increasing $[K^+]_o$ on the binding step XClo → XClKo (this modification amounts to suppressing this binding step with no modification of the other parameters) and by the addition of an inhibitory step $XClNH_4o \rightarrow XClNH_4Ko$, whose affinity constant for K^+_o, K_K, was 5, 10, or 15 mM (superposed traces), the greatest inhibition being for K_K = 5 mM.

mM NH_4^+, although larger than the inhibition in 2 mM NH_4^+, was not as markedly larger as in the experiments. Second, the increases in pH_i induced by rises in $[K^+]_o$ were slower than the experimental ones. Third, after returning to 10 mM K^+, the small rebound acidification present in the experimental records was not reproduced. A transporter model in which inhibition by extracellular K^+ was noncompetitive (Fig. 11 C, legend) corrected these failings, but excessively so. We did not attempt to fit the experimental data more precisely since our transporter model is highly simplified, but these comparisons to simulations do suggest that inhibition by extracellular K^+ may be partly noncompetitive.

DISCUSSION

Sensitivity to loop diuretics and external chloride (Marcaggi et al., 1999) indicate that the cotransporter studied belongs to the electroneutral cation-chloride cotransporter family (Haas and Forbush, 1998). Despite the electroneutrality of the process and the simultaneous flux of NH_3 across the membrane (Marcaggi et al., 1999), we have quantified the transport of NH_4^+ on the cotransporter after first measuring several parameters (buffering power, P_{NH3}...) that link the transmembrane flux of NH_4^+ to changes in pH_i.

Parameters for the Cell Model: pH_i, β_i, P_{NH3}

The null method of pH measurement used on the isolated bundles of glial cells showed that many bundles had pH_is at least as alkaline as those measured with pH microelectrodes in slices of retina (mean: 7.31; Coles et al., 1996), in agreement with the generally alkaline pH reported in many kinds of glial cells (see Deitmer and Rose, 1996). β_i [12.2 mequiv (pH unit · liter)$^{-1}$] is close to the value of 10.4 measured in snail neurons (Szatkowski and Thomas, 1989). Our estimate of P_{NH3} (13 $\mu m\ s^{-1}$) is well within the large range of values reported for biological membranes, which range from 108 $\mu m\ s^{-1}$ or higher in erythrocytes (Klocke et al., 1972; Labotka et al., 1995) to undetectably small at the apical membranes of colonic crypt cells (Singh et al., 1995). This variation appears in part to be correlated inversely with the density of proteins in the membrane: P_{NH3} is high in protein-free artificial membranes (Antonenko et al., 1997) and low in membranes of urinary bladder, which are densely packed with uroplakins (Chang et al., 1994). P_{NH3} has not, to our knowledge, been determined for cells of nervous tissue other than the bee retinal glial cells, so we do not know if our value is typical. From experiments similar to that of Fig. 6 B, we compared the permeabilities of the membrane to various neutral lipophilic compounds. We found that the permeabilities to the neutral forms of the amines TMA, MA, and ammonium or the carboxylic acids caproate, propionate, and acetate were greater the greater the hydrophobic part of the molecule (-CH_2- groups); i.e., $P_{TMA} > P_{MA} > P_{NH3}$ and $P_{caproate} > P_{propionate} > P_{acetate}$. Thus, it appears that the relative permeability of the cell membrane to these nonelectrolytes depends more on the hydrophobicity of the molecule than on its size, in accordance with Overton's rule (Overton, 1899).

Membrane Potential, Cl^- Gradient, and pH Regulation

A major difference, potentially important for certain cell functions, between the glial cells in the isolated bundles and those on which published results were obtained in slices of bee retina, is the apparent membrane potential. On the assumption that application of nigericin caused H^+ to distribute across the membrane with the same passive distribution as K^+, we concluded that mean V_m in the bundles was −4 mV. Support for a small V_m is given by the observation (Marcaggi et al., 1999) that in dissociations of the kind used here, rhodamine 123 selectively labeled photoreceptor cells. Since rhodamine 123 tends to partition preferentially into negatively charged compartments, this observation is compatible with the isolated bundles of glial cells having a membrane potential, V_m, much smaller than that of the photoreceptors. Despite the smallness of V_m, the glial cell bundles were able to regulate their pH_i and to recover from repeated acid loads, although slightly more slowly than the recovery from a stimulus-induced acidification of glial cells in slices (Coles et al., 1996). And in electrically functioning retinal slices, a wide range of glial cell membrane potentials have been recorded (−10 to −75 mV) with little apparent consequence for homeostasis of extracellular ions or metabolism (Bertrand, 1974; Coles et al., 1986; our unpublished observations). The mechanism of pH regulation in the bee glial cells is unknown and a mechanism not dependent on an ionic gradient is conceivable, as reported in C6 glial cells (Volk et al., 1998).

Transporters of the cation-Cl^- family are normally electroneutral, and the effect of ammonium on glial cell V_m in bee retinal slices is compatible with electroneutral transport (Coles et al., 1996), so V_m is expected to have no direct effect on the thermodynamics of the NH_4^+ transport. However, since Cl^- is distributed approximately passively (Coles et al., 1989), the concentration gradient is much greater in glial cells in vivo and it is predicted that uptake of NH_4^+ would be more effective than in the isolated bundles.

NH_4^+/K^+ Selectivity of the Transporter

Until now, the few studies of competition between K^+ and NH_4^+ for inward transport into animal cells on transporters have reported a selectivity for K^+ (Kinne et al., 1986; Cougnon et al., 1999). It has, however, been proposed that NH_4^+ transport is a physiologically significant process, notably in kidney cells (Good, 1994) and in salivary acinar cells (Evans and Turner, 1998). We have shown that for brief applications of ammonium in the millimolar range, the Cl^--dependent transport in bee retinal glial cells is functionally selective for NH_4^+ over K^+. Further, a minimal numerical model of the transport process in which NH_4^+ competes for a transporting site with an affinity approximately twice that for K^+ accounted for the main features of the pH_i responses not only for brief applications of ammonium but also for more complex protocols. Since K^+ is the physiological cation whose ionic radius is closest to that of NH_4^+ (Robinson and Stokes, 1959) and whose permeation through channels is most similar to that of NH_4^+ (Hille, 1992), it is unlikely that the transporter has as high an affinity for any other major physiological ion, and we conclude that it is selective for NH_4^+.

Reported values for K_m (K^+) calculated for K^+ influx by Cl^--dependent transport into erythrocytes are 55 mM (sheep; Delpire and Lauf, 1991) and 140 mM (human; Kaji, 1989). These values are higher than the K_i calculated in this study (10–27 mM) on the assumption (supported by the Lineweaver-Burke plots of Fig. 9, B and C) that the inhibition is purely competitive. However, if, as suggested by Fig. 11, the inhibition is partly noncompetitive, then the K_i for the competitive component will be higher and closer to the values for erythrocytes. Not only does the transporter on the bee retinal glial cell have a lower affinity for K^+ than for NH_4^+, but preliminary results suggest that even the K^+ that is bound may not be transported rapidly (Marcaggi and Coles, 1998).

Possible Advantages of Glial Uptake of Ammonium in the NH_4^+ Form

We have shown that ammonium enters bee retinal glial cells overwhelmingly in the NH_4^+ form. It is striking that this is also the case for mammalian astrocytes (at least those cultured from neonatal mice), although, in contrast to the bee glial cells, the NH_4^+ entry into cultured astrocytes appears to occur mainly through Ba^{2+}-sensitive channels (Nagaraja and Brookes, 1998; P. Sartor and P. Marcaggi, unpublished data). Entry of ammonium into cells is favored in two ways if it crosses the membrane as NH_4^+ instead of as NH_3. First, at physiological pHs, the majority of the ammonium is in the NH_4^+ form. Second, the entry can be coupled to a gradient. In the case of bee retinal cells in vivo, this is the Cl^- concentration gradient, and in cultured mouse astrocytes it is the electrical potential gradient.

A major ammonium-consuming process in bee retinal glial cells is the conversion of pyruvate to alanine (Tsacopoulos et al., 1994, 1997a). As a substrate, NH_4^+ will contribute to the regulation of the reactions (Tsacopoulos et al. 1997a,b). In addition, NH_4^+ allosterically activates phosphofructokinase (Lowry and Passoneau, 1966; Sugden and Newsholme, 1975), an effect that, in mammals, may contribute to the coupling of glutamate release by neurons to glycolysis in astrocytes proposed by Pellerin and Magistretti (1994) (see also Magistretti et al., 1999).

In the case of bee retinal glial cells, the ammonium

consumption can be summarized by the reaction: CH_3-CO-COO^- + NH_4^+ + NADH + H^+ → CH_3-$CHNH_3^+$-COO^- + H_2O + NAD^+.

Since this reaction consumes H^+, pH_i is better conserved if ammonium is supplied in the NH_4^+ form. In astrocytes, the pathways of energy metabolism are still a matter of debate (see, e.g., Demestre et al., 1997), but there, too, the proportion of ammonium that enters as NH_3 or NH_4^+ will affect pH homeostasis in the brain.

We thank Dr. Robert Dantzer for laboratory facilities and Jean-Louis Lavie for his contribution to the set up.

Financial support was received from the Conseil Régional d'Aquitaine (97-0301208).

Submitted: 5 November 1999
Revised: 10 May 2000
Accepted: 11 May 2000

REFERENCES

Abramowitz, M., and I.A. Stegun. 1965. Handbook of Mathematical Functions. Dover Publications Inc., New York, NY. 1046 pp.

Antonenko, Y.N., P. Pohl, and G.A. Denisov. 1997. Permeation of ammonia across bilayer lipid membranes studied by ammonium ion selective microelectrodes. *Biophys. J.* 72:2187–2195.

Benjamin, A.M., and J.H. Quastel. 1975. Metabolism of amino acids and ammonia in rat brain cortex slices *in vitro*: a possible role of ammonia in brain function. *J. Neurochem.* 25:197–206.

Bertrand, D. 1974. Etude des propriétés électrophysiologiques des cellules pigmentaires de la rétine du faux-bourdon (*Apis mellifera*). Thesis No. 1650. Université de Genéve.

Boron, W.F., and P. De Weer. 1976. Intracellular pH transients in squid axons caused by CO_2, NH_3, and metabolic inhibitors. *J. Gen. Physiol.* 67:91–112.

Boyarsky, G., M.B. Ganz, R.B. Sterzel, and W.F. Boron. 1988. pH regulation in single glomerular mesangial cells I. Acid extrusion in absence and presence of HCO_3^-. *Am. J. Physiol. Cell Physiol.* 255:C844–C856.

Boyarsky, G., C. Hanssen, and L.A. Clyne. 1996. Inadequacy of high K^+/nigericin for calibrating BCECF. *Am. J. Physiol. Cell Physiol.* 271:C1131–C1156.

Cardinaud, B., J.A. Coles, P. Perrottet, A.J. Spencer, M.P. Osborne, and M. Tsacopoulos. 1994. The composition of the interstitial fluid in the retina of the honeybee drone: implications for the supply of substrates of energy metabolism from blood to neurons. *Proc. R. Soc. Lond. B Biol. Sci.* 257:49–58.

Chang, A., T.G. Hammond, T.T. Sun, and M.L. Zeidel. 1994. Permeability properties of the mammalian bladder apical membrane. *Am. J. Physiol. Cell Physiol.* 267:C1483–C1492.

Coles, J.A., P. Marcaggi., and J.L. Lavie 1999. A rapid wavelength changer based on liquid crystal shutters for use in ratiometric microspectrophotometry. *Pflügers Arch.* 437:986–989.

Coles, J.A., P. Marcaggi, C. Véga, and N. Cotillon. 1996. Effects of photoreceptor metabolism on interstitial and glial cell pH in bee retina: evidence for a role for NH_4^+. *J. Physiol.* 495:305–318.

Coles, J.A., and R.K. Orkand. 1983. Modification of potassium movement through the retina of the drone (Apis mellifera male) by glial uptake. *J. Physiol.* 340:157–174.

Coles, J.A., R.K. Orkand, and C.L. Yamate. 1989. Chloride enters glial cells and photoreceptors in response to light stimulation in the retina of the honey bee drone. *Glia.* 2:287–297.

Coles, J.A., R.K. Orkand, C.L. Yamate, and M. Tsacopoulos. 1986. Free concentrations of Na, K and Cl in the retina of the honeybee drone: stimulus-induced redistribution and homeostasis. *Ann. NY Acad. Sci.* 481:303–317.

Coles, J.A., and R. Rick. 1985. An electron microprobe analysis of photoreceptors and outer pigment cells in the retina of the honey bee drone. *J. Comp. Physiol.* 156:213–222.

Cougnon, M., P. Bouyer, F. Jaisser, A. Edelman, and G. Planelles. 1999. Ammonium transport by the colonic H^+-K^+-ATPase expressed in *Xenopus* oocytes. *Am. J. Physiol. Cell Physiol.* 277:C280–C287.

Deitmer, J.W., and C.R. Rose. 1996. pH regulation and proton signalling by glial cells. *Prog. Neurobiol.* 48:73–103.

Delpire, E., and P.K. Lauf. 1991. Kinetics of Cl-dependant K fluxes in hyposmotically swollen low K sheep erythrocytes. *J. Gen. Physiol.* 97:173–193.

Demestre, M., M.G. Boutelle, and M. Fillenz. 1997. Stimulated release of lactate in freely moving rats is dependent on the uptake of glutamate. *J. Physiol.* 499:825–832.

Eisner, D.A., N.A. Kenning, S.C. O'Neill, G. Pocock, C.D. Richards, and M. Valdeolmillos. 1989. A novel method for absolute calibration of intracellular pH indicators. *Pflügers Arch.* 413:553–558.

Engasser, J.M., and C. Horvath. 1974. Buffer-facilitated proton transport pH profile of bound enzymes. *Biochim. Biophys. Acta.* 358:178–192.

Evans, R.L., and R.J. Turner. 1998. Evidence for physiological role of NH_4^+ transport on secretory Na^+-K^+-$2Cl^-$ cotransporter. *Biochem. Biophys. Res. Commun.* 245:301–306.

Good, D.W. 1994. Ammonium transport by the thick ascending limb of Henle's loop. *Annu. Rev. Physiol.* 56:623–647.

Haas, M., and B.R. Forbush. 1998. The Na-K-Cl cotransporters. *J. Bioenerg. Biomembr.* 30:161–172.

Hassel, B., H. Bachelard, P. Jones, F. Fonnum, and U. Sonnewald. 1997. Trafficking of amino acids between neurons and glia *in vivo*. Effects of inhibition of glial metabolism by fluoroacetate. *J. Cerebr. Blood Flow Metab.* 17:1230–1238.

Hille, B. 1992. Ionic Channels of Excitable Membranes. 2nd ed. Sinauer Associates, Inc., Sunderland, MA. 607 pp.

Jacobs, M.H. 1940. Some aspects of cell permeability to weak electrolytes. *Cold Spring Harbor Symp. Quant. Biol.* 8:30–39.

Kaiser, B.N., P.M. Finnegan, L.F. Whitehead, F.J. Bergersen, D.A. Day, and M.K. Udvardi. 1998. Characterization of an ammonium transport protein from the peribacteroid membrane of soybean nodules. *Science.* 281:1202–1206.

Kaji, D. 1989. Kinetics of volume-sensitive K transport in human erythrocytes: evidence for asymmetry. *Am. J. Physiol. Cell Physiol.* 256:C1214–C1223.

Kenyon, J.L., and W. R. Gibbons. 1977. Effects of low chloride solutions on action potentials of sheep cardiac purkinje fibers. *J. Gen. Physiol.* 70:635–660.

Kinne, R., E. Kinne-Saffran, H. Schütz, and B. Scholermann. 1986. Ammonium transport in medullary thick ascending limb of rabbit kidney: involvement of the Na^+, K^+, Cl^--cotransporter. *J. Membr. Biol.* 94:279–284.

Klocke, R.A., K.K. Andersson, H.H. Rotman, and R.E. Forster. 1972. Permeability of human erythrocytes to ammonia and weak acids. *Am. J. Physiol.* 222:1004–1013.

Labotka, R.J., P. Lundberg, and P.W. Kuchel. 1995. Ammonia permeability of erythrocyte membrane studied by ^{14}N and ^{15}N saturation transfer NMR spectroscopy. *Am. J. Physiol. Cell Physiol.* 268: C686–C699.

Lowry, O.H., and J.V. Passoneau. 1966. Kinetic evidence for multiple binding sites on phosphofructokinase. *J. Biol. Chem.* 241: 2268–2279.

Magistretti, P.J., L. Pellerin, D.L. Rothman, and R.G. Shulman. 1999. Energy on demand. *Science.* 283:496–497.

Marcaggi, P. 1999. Capture de NH_4^+ dans les cellules gliales de ré-

tine d'abeille par un transporteur membranaire spécifique. Thesis No. 698. Université Bordeaux 2.

Marcaggi, P., and J.A. Coles. 1998. The major routes of entry of NH_4^+ and K^+ into bee retinal glial cells are independent. *J. Physiol.* 513:15P–16P. (Abstr.)

Marcaggi, P., D.T. Thwaites, and J.A. Coles. 1996. Accumulation of protons in glial cells dissociated from bee retina in response to ammonium. *J. Physiol.* 495:60P. (Abstr.)

Marcaggi, P., D.T. Thwaites, J.W. Deitmer, and J.A. Coles. 1999. Chloride-dependent transport of NH_4^+ into bee retinal glial cells. *Eur. J. Neurosci.* 11:167–177.

Margolis, L.B., I.Y. Novikova, I.A. Rozovskaya, and V.P. Skulachev. 1989. K^+/H^+-antiporter nigericin arrests DNA synthesis in Ehrlich ascites carcinoma cells. *Proc. Natl. Acad. Sci. USA.* 86:6626–6629.

Nagaraja, T.N., and N. Brookes. 1998. Intracellular acidification induced by passive and active transport of ammonium ions in astrocytes. *Am. J. Physiol. Cell Physiol.* 43:C883–C891.

Nett, W., and J.W. Deitmer. 1996. Simultaneous measurements of intracellular pH in the leech giant glial cell using 2′,7′-bis-(2-carboxyethyl)-5,6-carboxyfluorescein and ion-sensitive microelectrodes. *Biophys. J.* 71:394–402.

Overton, E. 1899. Ueber die allgemeinen osmotischen Eigenschaften der Zelle, ihre vermutlichen Ursachen und ihre Bedeutung fur die Physiologie. *Vierteljahrsschr. Naturforsch. Ges. Zuerich.* 44:88–135.

Pellerin, L., and P.J. Magistretti. 1994. Glutamate uptake into astrocytes stimulates aerobic glycolysis: a mechanism coupling neuronal activity to glucose utilization. *Proc. Natl Acad. Sci. USA.* 91: 10625–10629.

Pressman, B.C., E.J. Harris, W.S. Jagger, and J.H. Johnson. 1967. Antibiotic-mediated transport of alkali ions across lipid barriers. *Proc. Natl. Acad. Sci. USA.* 58:1949–14956.

Race, J.E., F.N. Makhlouf, P.J. Logue, F.H. Wilson, P.B. Dunham, and E.J. Holtzman. 1999. Molecular cloning and functional characterization of KCC3, a new K-Cl cotransporter. *Am. J. Physiol.* 277:C1210–C1219.

Robinson, R.A., and R.H. Stokes. 1959. Electrolyte solutions. 2nd ed. London Butterworths, London, UK. 571 pp.

Roos, A., and W.F. Boron. 1981. Intracellular pH. *Physiol. Rev.* 61: 296–434.

Sanders, D., U.-P. Hansen, D. Gradmann, and C.L. Slayman. 1984. Generalized kinetic analysis of ion-driven cotransport systems: a unified interpretation of selective ionic effects on Michaelis parameters. *J. Membr. Biol.* 77:123–152.

Sillén, L.G. 1964. Stability constants of metal-ion complexes. I. Inorganic ligands. Chemical Society (Spec. Publ. 17.), London, UK. 150 pp.

Singh, S.K., H.J. Binder, J.P. Geibel, and W.F. Boron. 1995. An apical permeability barrier to NH_3/NH_4^+ in isolated, perfused colonic crypts. *Proc. Natl. Acad. Sci. USA.* 92:11573–11577.

Sugden, P., and E. Newsholme. 1975. The effect of ammonium, inorganic phosphate and potassium ions on the activity of phosphofructokinases from muscle and nervous tissues of vertebrates and invertebrates. *Biochem. J.* 150:113–122.

Szatkowski, M.S., and R.C. Thomas. 1989. The intracellular H^+ buffering power of snail neurones. *J. Physiol.* 409:89–101.

Thomas, J.A., R.N. Buchsbaum, A. Zimniak, and E. Racker. 1979. Intracellular pH measurements in Ehrlich ascites tumor cells utilizing spectroscopic probes generated *in situ*. *Biochemistry.* 18: 2210–2218.

Thomas, R.C. 1984. Experimental displacement of intracellular pH and the mechanism of its subsequent recovery. *J. Physiol.* 354:3P–22P.

Tsacopoulos, M., C.L. Poitry-Yamate, and S. Poitry. 1997a. Ammonium and glutamate released by neurons are signals regulating the nutritive function of a glial cell. *J. Neurosci.* 17:2383–2390.

Tsacopoulos, M., C.L. Poitry-Yamate, S. Poitry, P. Perrottet, and A.L. Veuthey. 1997b. The nutritive function of glia is regulated by signals released by neurons. *Glia.* 21:84–91.

Tsacopoulos, M., A.L. Veuthey, G. Saravelos, P. Perrottet, and G. Tsoupras. 1994. Glial cells transform glucose to alanine which fuels the neurons in the honeybee retina. *J. Neurosci.* 14:1339–1351.

Volk, C., T. Albert, and O.S. Kempski. 1998. A proton-translocating H^+-ATPase is involved in C6 glial pH regulation. *Biochim. Biophys. Acta.* 1372:28–36.